

# Representation of transport and scavenging of trace particles in the Emanuel moist convection scheme

Romain Pilon<sup>1,2</sup>, Jean-Yves Grandpeix<sup>1</sup> and Philippe Heinrich<sup>2</sup>

<sup>1</sup>Laboratoire de Météorologie Dynamique, Paris, France

<sup>2</sup>Commissariat à l'Énergie Atomique DAM-Ile de France, 91297 Arpajon cedex, France

\*Correspondence to: Laboratoire de Météorologie Dynamique, Boîte Postale 99, 4 Place Jussieu 75252 Paris Cedex 5, romain.pilon@lmd.jussieu.fr

In the Tropics, cumulus convection has a major influence on precipitation and vertical transport of atmospheric particles, which are subject to scavenging by precipitation. A new parameterization of transport and scavenging of trace particles by convective clouds and precipitation has been developed and introduced in the Laboratoire de Météorologie Dynamique general circulation model (LMDz). This model uses the deep convection scheme of Emanuel, which is particularly suited for tropics. Our parameterization of transport and scavenging is closely linked to this scheme and our developments follow step-by-step the building of this convection representation. The purpose of this study is to understand better the influence of convection on the tracer vertical distribution and to assess the role of the convection parameterization.

Short term and long term simulations have been performed focusing on the concentrations of the natural radionuclide <sup>7</sup>Be, which is produced mainly in the stratosphere and upper troposphere and attaches to available aerosols. Single-column simulations forced by data from Tropical Ocean-Global Atmosphere-Coupled Ocean-Atmosphere Response Experiment (TOGA COARE) show the high efficiency of in-cloud scavenging by convective and large-scale processes on the removal of the tracer. These simulations show that, in the LMDz model, convection does not affect radionuclide concentrations as much as stratiform clouds and associated precipitation. In the free troposphere and in the boundary layer, below-cloud evaporation of rain has a major effect on tracer distribution, unlike impaction, which has a negligible effect. Three-dimensional model simulation results are compared to surface data of a station belonging to the worldwide network of the Comprehensive Nuclear-Test-Ban Treaty Organization (CTBTO). We show that this new parameterization is able to reproduce the observed yearly averaged concentrations of <sup>7</sup>Be at the surface and decrease by a third the overestimation of radionuclides formerly simulated without convective scavenging. LMDz simulations have been also performed over the 2007 year at a global scale using the terragenic <sup>210</sup>Pb and cosmogenic <sup>7</sup>Be radionuclides. Copyright © 2013 Royal Meteorological Society

*Key Words:* parameterization, deep convection, scavenging, transport, radionuclide, climate model

This article has been accepted for publication and undergone full peer review but has not been through the copyediting, typesetting, pagination and proofreading process, which may lead to differences between this version and the Version of Record. Please cite this article as doi: 10.1002/qj.2431

## 1. Introduction

In the Tropics, deep convection has a substantial influence on large-scale circulation and on water distribution in the troposphere. Moreover it greatly impacts aerosol vertical distribution, which is not only controlled by air transport but also by scavenging, the cleansing of material from the atmosphere by hydrometeors. In the last two decades, the complexity and realism of the representation of this process in climate models has been increasing. However, representations of scavenging differ from a general circulation model (GCM) to another. As reported in [Rasch et al. \(2000\)](#), results from model intercomparison underline uncertainties, which come from either transport and scavenging parameterizations or deep convective cloud parameterization (see [Mahowald et al. 1995; Tost et al. 2006, 2010](#)). Nevertheless [Koch et al. \(1996\)](#), [Liu et al. \(2001\)](#) or [Heinrich and Jamelot \(2011\)](#) note that the surface concentration  ${}^7\text{Be}$  in the tropics is generally overestimated owing to insufficient scavenging within convective clouds or removal by precipitation. So far, the parameterization of wet removal by convective clouds and precipitation distinguishes in-cloud scavenging, below-cloud impaction, release by evaporation. Representation of scavenging processes is generally based on prescribed in-cloud scavenging ratios and implicitly parameterizes nucleation and impaction processes using the formulation of [Giorgi and Chameides \(1986\)](#). Some authors separate in-cloud scavenging with scavenging in convective updraft ([Lawrence and Rasch 2005](#)). Some calculate below-cloud impaction and release by evaporation using constant rates or depending on precipitation and evaporation rates ([Liu et al. 2001; Reddy and Boucher 2004](#)), while others use complex formulation of microphysics in the effort to gain accuracy ([Andreae and Rosenfeld 2008; Croft et al. 2010](#)).

Here, our approach is to develop a parameterization based on the moist convective scheme of [Emanuel \(1991\)](#). The main asset of this scheme is the precipitating downdrafts, which are greatly involved in deep convective processes. It is a feature expected to play a key role for tracers originating in the upper troposphere such as  ${}^7\text{Be}$ . The parameterization is expected to provide a feedback on the moist convective scheme parameters such as the fractional area covered by these precipitating downdrafts. The new parameterization follows closely the physical mechanisms of Emanuel scheme, the processes in the drafts of the deep convection and exchanges between them at each level.

The model used for this study is the GCM LMDZ ([Hourdin et al. 2006](#)), more specifically its version used for the third Coupled Model Intercomparison Project (CMIP3) simulations. In this model moist processes are represented by two parameterizations: deep convection ([Emanuel 1991](#)) and large-scale condensation processes ([Le Treut and Li 1991](#)). Our approach is to deal separately with the tracer transport and scavenging associated with these two schemes: (i) for the large-scale condensation we keep a standard description comprising three parts, in-cloud scavenging, below cloud scavenging and release by rain evaporation; the corresponding schemes are briefly described in the

appendix; (ii) for the deep convection we designed a new parameterization, which accounts for transport as well as scavenging in the various vertical drafts.

An overview of the existing scavenging parameterizations in the LMDz climate model is provided in [Heinrich and Jamelot \(2011\)](#). The simulations use the natural radionuclide  ${}^7\text{Be}$  as a passive tracer for assessing our parameterization. Associated with the  ${}^{210}\text{Pb}$  radionuclide,  ${}^7\text{Be}$  has been widely used to evaluate atmospheric transport and aerosol removal processes in GCMs ([Balkanski et al. 1993; Koch et al. 1996; Liu et al. 2001](#)). Thanks to the low (high) altitude of the tropospheric source of  ${}^{210}\text{Pb}$  ( ${}^7\text{Be}$ ) the combined study of these tracers is particularly interesting in the tropics to analyze the role of scavenging by large-scale and convective processes.

The aim of this research is to diagnose how the processes in deep convection influence the vertical tracers distribution and its elimination by precipitation.

The present paper is devoted to the presentation of this new scavenging parameterization coupled with the Emanuel convective scheme. The formulation of the transport and scavenging model is presented in section 2. Section 3 evaluates the scheme in a single-column model simulation (SCM). In section 4 the parameterization is tested in the GCM LMDz at a global scale and results are compared with observations at a tropical station. Lastly, we summarize and discuss the features of this new scavenging scheme.

## 2. Model description

The new parameterization of transport and scavenging describes the redistribution and the removal of tracers in deep convective clouds by rain inside and below the clouds. It is tested in the LMDz general circulation model. It is implemented within the Emanuel convection scheme (see [Emanuel 1991; Emanuel and Živković-Rothman 1999](#)).

The presentation of our scheme follows the one of [Emanuel \(1991\)](#) and we use the same notations for mass fluxes. The only difference is that all fluxes are defined as a function of continuous vertical levels  $z$  instead of discrete layers. The parameterization of transport and scavenging is separated into two parts: transport and scavenging in the saturated updrafts and downdrafts, and transport and scavenging in the unsaturated downdrafts. (We shall not use the usual terms of “in-cloud” and “below-cloud” scavenging since, in the Emanuel parameterization, a fraction of the precipitation falls through the cloud). In the study, the moist convective scheme does not include ice thermodynamics, which could affect the role of convective precipitation in the upper troposphere. However, as noted by [Liu et al. \(2001\)](#), observations ([Jacob 2000](#)) show that within the convective updrafts aerosols incorporated into the cloudy air are incorporated in condensed phase of water irrespective of the nature of the condensed phase.

The effect of the deep convective cloud on the environmental tracer distribution  $\tilde{C}$  is split into two tendencies,  $(\partial_t \tilde{C})_{sat}$  and  $(\partial_t \tilde{C})_{unsat}$  induced by saturated drafts and unsaturated drafts on the environment, respectively:

$$(\partial_t \tilde{C})_{cv} = (\partial_t \tilde{C})_{sat} + (\partial_t \tilde{C})_{unsat}, \quad (1)$$

where  $\tilde{C}$  is the tracer number concentration in the environment. In each tendency is included the mass balancing displacement as in Emanuel scheme. This splitting allows a separation of the processes i.e. the amount of tracers coming from  $(\partial_t \tilde{C})_{sat}$  comes from the saturated processes and the one coming from  $(\partial_t \tilde{C})_{unsat}$  comes from the evaporation of precipitation and from the detrainment of precipitating downdraft into the environment. The parameterizations of each tendency is detailed in sections 2.4 and 2.5.

### 2.1. Short description of Emanuel scheme

The representation of convection follows the scheme of Emanuel (1991) and is based on the idea that convective clouds are not homogeneous in nature: the cloud is represented by multiple vertical drafts moving adiabatically between levels where mixing with environmental air occurs.

Air below the cloud base ascends adiabatically, forming updrafts, and lifts unmixed up to some level  $z'$ , between the cloud base and the level of neutral buoyancy. At each level  $z'$ , a fraction  $\epsilon(z')$  of condensed water ( $l_a$ ) produced during the ascent is converted into precipitation, and is defined by Emanuel (1991) such that  $\epsilon(z)$  is varying linearly from 0 to  $\epsilon_{max}$  between 150 hPa and 500 hPa above the lifting condensation level (LCL), and is constant elsewhere.

The maximum precipitation efficiency is a bit less than the unity (0.999) to allow cloud water to remain in suspension in the upper troposphere (Bony and Emanuel 2001). The air from the adiabatic updraft, whose liquid water content is now  $(l_a(1 - \epsilon(z')))$  is mixed at level  $z'$  with environmental air yielding a spectrum of mixtures. Each mixture moves adiabatically up or down to its level  $z$  ( $z$  can be higher or lower than  $z'$ ) of neutral buoyancy – in ascending mixtures, water may further condensate and precipitate – and then, after removal of precipitation, detains in the environment.

Precipitation formed in adiabatic ascents and in the mixtures is added to a single precipitating downdraft driven by the evaporation of the rain.

Deep convective clouds cover an area smaller than the grid cell  $S_t$ . When precipitation occurs, it forms the precipitating downdraft covering a region  $S_d$ . The fractional area covered by the unsaturated downdraft  $\sigma_d = S_d/S_t$  is prescribed by Emanuel: the draft covers only 1% of the grid cell, a smaller region compared with large-scale clouds and precipitation, which may cover a major fraction of grid cell. In these spatial coverages aerosols would be less subject to removal by convective precipitation than large-scale precipitation.

### 2.2. Assumptions on aerosols

LMDz climate model does not yet distinguish the different aerosol modes. The tracers used this study are radionuclides  $^{210}\text{Pb}$  and  $^7\text{Be}$ , which attach themselves to all available submicrometric hydrophilic aerosols of the accumulation mode (Bondietti et al. 1987). In addition,  $^{210}\text{Pb}$  also attaches itself to

hydrophobic aerosols according to its concentrations. From that perspective, we treat  $^{210}\text{Pb}$  like  $^7\text{Be}$  and a monodisperse distribution size is considered. Furthermore, in the model all aerosol particles act as condensation nuclei irrespective of the temperature. According to the sizes of aerosols, which bear these two radionuclides (Bondietti et al. 1987; Winkler et al. 1998; Marley et al. 2000), they belong to the Greenfield gap thus in the accumulation mode and as we use a monodisperse distribution for aerosols, Brownian motion and inertial impaction processes can be neglected (Greenfield 1957). For simplicity, we did not parameterize these processes.

### 2.3. Notations and conventions

In order to simplify the writing of following equations, we use a specific notation. Let us note  $C_x^y$  the amount of tracer per unit of mass of the phase  $x$  ( $c$  for cloudy condensate,  $p$  for precipitating water and  $v$  for air/vapor mixture) in draft  $y$  ( $a$  for adiabatic ascent,  $m$  for the mixed drafts,  $d$  for the saturated downdraft,  $u$  for the saturated updraft and  $p$  for precipitating downdraft). In the case of radionuclides, the amount of tracer is measured by its activity (as is usual in literature). The quantity  $C_x^y$  is hereafter called tracer concentration.

We use  $M$  to represent mass fluxes:  $M_a$  for the adiabatic updraft,  $\tilde{M}$  for the environment,  $M_p$  for the precipitating downdraft;  $\frac{\partial M_a}{\partial z} \delta z$  is the mass flux of the adiabatic draft ending in the layer  $[z, z + \delta z]$ .  $\frac{\partial M_m}{\partial z \partial z'} \delta z \delta z'$  is the mass flux of the mixed draft going from layer  $[z', z' + \delta z']$  to  $[z, z + \delta z]$ . All mass fluxes are defined positive upward.

Variables related to drafts going from  $z'$  to  $z$  are indexed  $zz'$ ; e.g.  $F^{zz'}$  is the fraction of environment air entrained at  $z'$  in the draft going to  $z$ .  $z_b$  is the altitude of cloud base and  $z_t$  the one of the cloud top. More generally, all variables with a tilde refer to the environment.

### 2.4. Saturated updrafts and downdrafts

In this section, we describe the transport and scavenging of tracers in the saturated drafts of the deep convective cloud.

The tendency of tracer concentration induced by saturated draft in the environment is the sum of the effects of entrainment, detrainment and the convergence of the subsiding mass flux  $\tilde{M}\tilde{C}$ :

$$\rho (\partial_t \tilde{C})_{sat} = d_C - e_{\tilde{C}} - \frac{\partial(\tilde{M}\tilde{C})}{\partial z}, \quad (2a)$$

where  $d_C$  and  $e_{\tilde{C}}$  are the fluxes of tracers in the detrainment and in the entrainment, respectively, and  $\rho$  the density of air. Using the environment mass budget equation  $\partial_z \tilde{M} = d - e$  where  $d$  and  $e$  are the detrained and the entrained mass fluxes, and assuming that tracer concentration in entrained air is equal to  $\tilde{C}$ , one may simplify (2a) into:

$$\rho (\partial_t \tilde{C})_{sat} = d_C - d\tilde{C} - \tilde{M} \frac{\partial \tilde{C}}{\partial z}, \quad (2b)$$

where the mass flux of detrained tracers  $d_C$  still needs to be defined. To calculate the tendency  $d_C$ , the contribution of each draft is calculated separately, considering the condensed phase and the vapor phase.

We assume thereafter that the fraction of tracers included in the vapor phase is constant along adiabatic displacements, i.e. after initiation of condensation no further activation occurs.

**Adiabatic ascent** Adiabatic ascent is fed by tracers in the layer going from the surface to an altitude  $h_s$  ( $h_s = 100\text{m}$ ) below  $z_b$ , the cloud base. The tracer concentration within this flux is given by:

$$C^a = \frac{1}{h_s} \int_0^{h_s} \tilde{C}(z) dz . \quad (3)$$

Air and tracers are lifted unmixed from the cloud base to an arbitrary level  $z'$  between the cloud base and the level of neutral buoyancy. During the ascent, a fraction  $\alpha_a$  of tracers serving as cloud condensation nuclei (CCN) is supposed to be activated into droplets and incorporated within cloud water.  $(1 - \alpha_a)$  stays in vapor. At  $z'$ , when adiabatic updraft stops, a fraction  $\epsilon(z')$  of cloud water precipitates, which removes  $\epsilon(z') \alpha_a$  of the tracers.

**Mixture** Remaining cloudy air, with tracer concentration  $C^a (1 - \epsilon(z') \alpha_a)$ , is mixed at level  $z'$  with environmental air before being displaced to  $z$ . Upon mixing with adiabatic ascent air, a fraction  $\beta_m$  of the CCN present in the entrained air is activated while  $(1 - \beta_m)$  stays in the vapor phase. As concerns air coming from the adiabatic ascent, we assume that tracers, which belonged to the condensed phase and the gaseous phase before mixing also belong to the condensed and gaseous phase respectively after mixing.

Then the amount of tracer in the condensed phase of a mixture of mass  $\delta m_m$  formed at level  $z'$ , going to level  $z$  and made of a fraction  $F^{zz'}$  of environment air and  $(1 - F^{zz'})$  of adiabatic ascent air is  $\delta m_m [(1 - \epsilon(z')) \alpha_a C^a (1 - F^{zz'}) + \beta_m \tilde{C}(z') F^{zz'}]$ . Since the amount of tracer present in the condensed phase is constant under adiabatic displacement, this is also equal to the amount of tracer present in the condensed phase when the mixture reaches level  $z$ :  $\delta m_m C_c^m(z, z') l_m^{zz'}$ . Hence the concentration of tracer in the condensed phase at level  $z$  reads:

$$C_c^m(z, z') = [(1 - \epsilon(z')) \alpha_a C^a (1 - F^{zz'}) + \beta_m \tilde{C}(z') F^{zz'}] / l_m^{zz'} , \quad (4a)$$

Likewise, the concentration in the vapor phase reads:

$$C_v^m(z, z') = [(1 - \alpha_a) C^a (1 - F^{zz'}) + (1 - \beta_m) \tilde{C}(z') F^{zz'}] / (1 - l_m^{zz'}) . \quad (4b)$$

According to their buoyancy, mixtures either descend or ascend to a level  $z$ . Descending mixtures (saturated

downdraft) are detrained without further precipitation formation. Amount of detrained tracer is then the sum of the amount of tracer in the two water phases. The tracer concentration in the saturated downdraft is

$$C^d(z, z') = \tilde{C}(z') F^{zz'} + (1 - F^{zz'}) (C^a - \epsilon(z') \alpha_a C^a) . \quad (5a)$$

If mixtures ascend, additional condensation is produced ( $l_m^{zz'}$ ) and might precipitate. A fraction  $\epsilon_m$  of condensed water is converted into precipitation at  $z$  in these mixtures. Then  $(1 - \epsilon_m)$  is the fraction of water detrained to  $z$  without precipitating. After precipitation formation, there remains  $C^u$  in the saturated updraft:

$$C^u(z, z') = C_v^m(z, z') (1 - l_m^{zz'}) + (1 - \epsilon_m^{zz'}) C_c^m(z, z') l_m^{zz'} , \quad (5b)$$

and  $\epsilon_m$  is given by:

$$\epsilon_m^{zz'} = \sup(0, 1 - (1 - \epsilon(z)) l_a(z)) / l_m^{zz'} , \quad (6)$$

where  $(1 - \epsilon(z)) l_a(z)$  is the remaining condensate in the adiabatic ascent at  $z$  after precipitation removal.

**Precipitation** Tracers in water converted into precipitation, at the end of the adiabatic ascent and within the mixtures, are further injected into the precipitation of the unsaturated downdraft (see section 2.4). The tracer concentrations in the precipitation do not play any role in the determination of  $(\partial_t \tilde{C})_{sat}$  but will be important later for the determination of  $(\partial_t \tilde{C})_{unsat}$  (sec 2.5).

Using  $l_a$ ,  $l_m^{zz'}$ ,  $\epsilon(z)$  and  $\epsilon_m^{zz'}$  make it possible to determine tracer concentration in the precipitation associated with the adiabatic ascent or with the mixtures. The concentration of tracer into the precipitation coming from the adiabatic ascent,  $C_p^a$ , may be written as:

$$C_p^a(z) = \frac{\alpha_a C^a}{l_a(z)} . \quad (7)$$

The concentration,  $C_p^m(z)$ , in the condensed water converted into precipitation (mixed at  $z'$  and displaced to  $z$ ) within all mixed drafts arriving in  $z$  may be written:

$$C_p^m(z) = \frac{\int_{z_b}^z C_c^m(z, z') \epsilon_m^{zz'} l_m^{zz'} \frac{\partial^2 M_m}{\partial z \partial z'} dz' dz}{\int_{z_b}^z \epsilon_m^{zz'} l_m^{zz'} \frac{\partial^2 M_m}{\partial z \partial z'} dz' dz} . \quad (8)$$

**Final formulation** The flux of tracer detrained at level  $z$  takes account of both concentrations  $C^d$  (Eq. 5a) and  $C^u$  (Eq. 5b) and is given by

$$\begin{aligned} d_C(z)dz &= \int_{z_b}^z \frac{\partial^2 M_m}{\partial z \partial z'} C^u(z', z) dz' dz \\ &\quad + \int_z^{z_t} \frac{\partial^2 M_m}{\partial z \partial z'} C^d(z', z) dz' dz . \end{aligned} \quad (9a)$$

The detrained mass flux reads:

$$d(z)dz = \int_{z_b}^{z_t} \frac{\partial^2 M_m}{\partial z \partial z'} dz' dz . \quad (9b)$$

Using (9a) and (9b) with (2b), with some algebra, the tendency induced by the saturated draft is

$$\begin{aligned} \rho (\partial_t \tilde{C})_{sat} &= (C^a - \tilde{C}(z)) \int_{z_b}^{z_t} \frac{\partial^2 M_m}{\partial z \partial z'} (1 - F^{zz'}) dz' \\ &\quad + \int_{z_b}^{z_t} \frac{\partial^2 M_m}{\partial z \partial z'} F^{zz'} (\tilde{C}(z') - \tilde{C}(z)) dz' \\ &\quad - \tilde{M} \frac{\partial \tilde{C}}{\partial z} + \rho (\partial_t \tilde{C})_{scav} , \end{aligned} \quad (10a)$$

where the first term corresponds to tracers in the mass flux supplied by the adiabatic ascent to the mixtures, the second one to tracers in the mass flux taken from the environment to the mixtures,  $\tilde{M} \frac{\partial \tilde{C}}{\partial z}$  is the compensating subsidence and the last term is the tendency induced by the scavenging, which is

$$\begin{aligned} \rho (\partial_t \tilde{C})_{scav} &= -\alpha_a C^a \int_{z_b}^{z_t} \frac{\partial^2 M_m}{\partial z \partial z'} (1 - F^{zz'}) \epsilon(z') dz' \\ &\quad - \alpha_a C^a \int_{z_b}^z \frac{\partial^2 M_m}{\partial z \partial z'} (1 - F^{zz'}) \epsilon_m^{zz'} (1 - \epsilon(z')) dz' \\ &\quad - \beta_m \int_{z_b}^{z_t} \frac{\partial^2 M_m}{\partial z \partial z'} F^{zz'} \epsilon_m^{zz'} \tilde{C}(z') dz' . \end{aligned} \quad (10b)$$

The first term corresponds to tracers removed by precipitation formation in the adiabatic ascent, the second one to tracers originating from the adiabatic ascent removed inside the mixtures and the last one to tracers of the environment removed by precipitation formation inside the mixtures.

If deep convective scavenging is disabled,  $(\partial_t \tilde{C})_{scav} = 0$ . Tracers are only transported by air flow without being transformed into CCN.

## 2.5. Unsaturated downdrafts

Following Emanuel, the unsaturated downdraft is separated into two parts: the precipitating water on one hand, and the air flowing down in the draft on the other hand, the latter being partly cloudy and partly clear. Falling precipitation evaporates into the clear air.

For simplicity, the air flowing down in the draft is called unsaturated air.

Within a layer at level  $z$ , with thickness  $\delta z$ , as depicted in Figure 1, precipitation flux  $P$  (precipitation per unit area of the model grid) is fed by precipitation formed from water condensed within the adiabatic ascent  $\frac{\partial P_a}{\partial z} \delta z$ , and within mixed drafts  $\frac{\partial P_m}{\partial z} \delta z$ . The

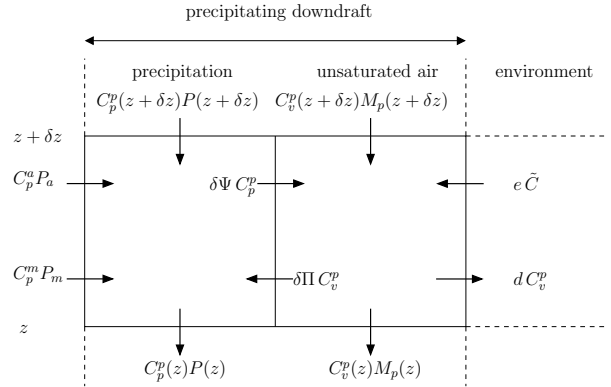


**Figure 1.** Sketch of an unsaturated downdraft and exchanges of tracers between precipitation, unsaturated air and environment.

two sources of precipitation  $\frac{\partial P_a}{\partial z} \delta z$  and  $\frac{\partial P_m}{\partial z} \delta z$  can be expressed in terms of the mass fluxes of the updrafts reaching that layer ( $\frac{\partial M_a}{\partial z} \delta z$  for the adiabatic ascent and  $\int_{z_b}^z \frac{\partial^2 M_m}{\partial z \partial z'} dz' \delta z$  for the mixed updrafts), of their condensed water content  $l_a$  and  $l_m^{zz'}$  and of the rates of conversion into precipitation  $\epsilon(z')$  and  $\epsilon_m^{zz'} l_m^{zz'}$ :

$$\frac{\partial P_a}{\partial z} \delta z = \frac{\partial M_a}{\partial z} \delta z \epsilon(z) l_a(z) , \quad (11a)$$

and

$$\frac{\partial P_m}{\partial z} \delta z = \int_{z_b}^z \frac{\partial^2 M_m}{\partial z \partial z'} \epsilon_m^{zz'} l_m^{zz'} dz' \delta z . \quad (11b)$$

Precipitation has a major influence on the tracers distribution in the environment. Let  $\delta\Psi$  be the mass of evaporated water in a given layer  $[z, z + \delta z]$  per unit time within the fractional area covered by the downdrafts  $\sigma_d$ . This mass can only evaporate within the fraction  $\sigma_s$  of precipitation falling in clear air:  $\delta\Psi = \sigma_s \sigma_d E \rho \delta z$ , where  $E$  is the evaporation rate (see Eq. 12b from Emanuel (1991)). Thus evaporation of precipitation increases by  $\delta\Psi C_p^p$  ( $C_p^p$  is the tracer concentration in the precipitation) the tracer amount in the unsaturated air  $\rho \delta z C_v^p$ .

Let  $\delta\Pi$  be the effective mass of the precipitating downdraft swept by the rain in the same layer per unit time within  $\sigma_d$ :  $\delta\Pi = \sigma_d \Lambda \rho \delta z$ , where  $\Lambda$  is the scavenging coefficient described hereinafter. Raindrops impact aerosols and remove  $\delta\Pi C_v^p$  tracers from the unsaturated air. Moreover, the unsaturated downdraft exchanges tracers with the environment by entrainment and detrainment according to the entrained mass flux  $e$  and the detrained mass flux  $d$ , respectively.

We calculate a tendency in which all above mentioned exchanges are represented to determine effects

of the unsaturated downdraft on the environment. This tendency,  $\partial_t C_{unsat}$ , is given by

$$\rho (\partial_t \tilde{C})_{unsat} = d C_v^p - e \tilde{C} - \frac{\partial \tilde{M} \tilde{C}}{\partial z}, \quad (12a)$$

Since the environmental mass flux  $\tilde{M}$  is equal to the opposite of the unsaturated downdraft mass flux  $M_p$  and as  $\partial_z \tilde{M} = e - d$ , the tendency may be written:

$$\rho (\partial_t \tilde{C})_{unsat} = d (C_v^p - \tilde{C}) + M_p \partial_z \tilde{C}. \quad (12b)$$

where  $M_p \partial_z \tilde{C}$  denotes the transport in the compensating ascent induced by the unsaturated downdraft.

To solve (12b) the tracer concentration in unsaturated air  $C_v^p$  is required. As the unsaturated draft is a steady system for each layer  $[z, z + \delta z]$ , budget equations can be established to describe the evolution of the draft. It is a two-way exchange of mass between precipitation, unsaturated air and environmental clear air, as shown on Figure 1, taking into consideration the water phase change. The amount of tracer in the precipitation between  $z$  and  $z + \delta z$  takes into account the variation of the flux of tracer transported by the precipitation ( $-\partial_z (P C_p^p) \delta z$ ). It is enriched by those in the sources of precipitation ( $+\partial_z P_a C_p^a \delta z$  and  $+\partial_z P_m C_p^m \delta z$ ) and by tracer of the unsaturated air impacted by the precipitation ( $+\delta \Pi C_v^p$ ); it is impoverished when tracers are released by evaporation of the precipitation ( $-\delta \Psi C_p^p$ ). On the other side, the amount of tracer in the precipitating downdraft takes into account of the variation of tracer in unsaturated air ( $-\partial_z (M_p C_v^p)$ ). Precipitating downdraft is driven by the evaporation of the precipitation, enriching the unsaturated air of  $+\delta \Psi C_p^p$  tracers, and this process therefore controls the entrainment (enrichment) of environment tracers ( $+e \delta z \tilde{C}$ ) and the detrainment (impoverishment) of tracers of the unsaturated air to the environment ( $-d \delta z C_v^p$ ). Moreover, precipitation impaction reduces the concentration within the unsaturated air ( $-\delta \Pi C_v^p$ ).

Summing up these various exchanges yields the following first order differential equation for  $C_p^p(z)$  and  $C_v^p(z)$  with top boundary conditions  $C_p^p(z_t) = C_v^p(z_t) = 0$ :

$$\begin{cases} -\partial_z (P C_p^p) + \partial_z P_a C_p^a + \partial_z P_m C_p^m \\ \quad -d\Psi/dz C_p^p + d\Pi/dz C_v^p = 0 \\ -\partial_z (M_p C_v^p) + e \tilde{C} - d C_v^p \\ \quad +d\Psi/dz C_p^p - d\Pi/dz C_v^p = 0. \end{cases} \quad (13)$$

If scavenging is disabled i.e. if tracers are transported only by the air flow of the unsaturated downdraft, terms related to the precipitation and evaporation are not involved in the system of equations (13) which becomes:

$$e \tilde{C} - d C_v^p = \partial_z (M_p C_v^p). \quad (14)$$

In this case the environmental tracer distribution is consequently closely related to the compensating ascent rather than the precipitation.

### Impaction scavenging coefficient: $\Lambda$

Usually, impaction by rain is represented by a coefficient calculated using a collision efficiency, which implicitly takes into account several microphysical processes (see Sportisse 2007). This latter coefficient is defined for monodisperse or polydisperse raindrops as well as for a particle size distribution (for instance Mircea et al. (2000)). Collision efficiency includes impaction split in three processes which are particle size-dependent: Brownian diffusion, interception and inertial impaction (Slinn 1983), for ultrafine, fine and coarse particles, respectively. The scavenging coefficient is proportional to the collision efficiency, to the raindrops and particles sizes as well as to the raindrops terminal velocity.

For simplicity, in our parameterization, as we consider only deep convection and associated rains, we neglect the Brownian diffusion and the inertial impaction. We assume that the impaction efficiency,  $\mathcal{E}_{imp}$ , is set to  $10^{-3}$  (as standard value for the range of the size of studied particles, i.e.  $[0.6 - 1] \mu\text{m}$ ). We also assume that, following Emanuel (1991), the rain velocity is equal to its terminal velocity  $w_t$  set to  $45 \text{ Pa.s}^{-1}$ . We use a monodisperse size distribution for raindrops: the raindrop diameter is set at 2 mm (value from Pruppacher and Klett (1996), for a tropical storm with heavy rainfall over Hawaii).

The temporal variation of mass of tracers removed from the unsaturated downdraft air ( $\frac{d\Pi}{dz} C_v^p = -\rho (\partial_t C_v^p)_{imp}$ ) is the temporal variation of the mass of tracers in the volume swept by  $n_d$  falling raindrops in the precipitating column over the surface covered by the downdraft, and is given by:

$$\rho (\partial_t C_v^p)_{imp} = -\rho C_v^p n_d \mathcal{E}_{imp} w_t \pi r^2. \quad (15)$$

where  $r$  is the radius of raindrops.

This equation can be related to the Emanuel scheme using the precipitation flux  $P$ . Indeed the precipitation flux combined with the flux of falling raindrop may be written :

$$P = \frac{4}{3} \pi r^3 n_d w_t \rho_l \sigma_d, \quad (16)$$

with  $\rho_l$  the density of liquid water. Thus, using (15) together with (16), we obtain

$$\rho (\partial_t C_v^p)_{imp} = -\Lambda \rho C_v^p, \quad (17a)$$

where the scavenging coefficient  $\Lambda$  is:

$$\Lambda = \mathcal{E}_{imp} \frac{3 P}{4 \rho_l \sigma_d r} \quad (17b)$$

In our model, precipitation has the same effect on tracers when falling through saturated air, unsaturated air and clear air, thus  $\Lambda$  is independent of the fraction of precipitation falling in clear air  $\sigma_s$ .

### 2.6. Sum up

The convective transport scheme is now complete: the resolution of the first order differential equation (13) associated with the diagnostic variable  $\Lambda$  (17b) allows

us to determine (12b); combined with (2a) (composed of (10a) and (10b)), the final solution of the tendency of tracer concentration induced by the convection (1) can be solved. In-cloud scavenging is characterized by two parameters representing two microphysical properties: CCN activation in adiabatic ascent and mixtures,  $\alpha_a$  and  $\beta_m$ , respectively. Impaction by rain depends on the collision efficiency parameter  $\varepsilon_{imp}$ .

The tracer sink in the saturated draft tendency (10b) is equal to the tracer source for the unsaturated downdrafts. The latter redistribute these tracers partly in the atmosphere, partly at the surface.

The discretization uses a staggered grid for the mass and precipitation fluxes,  $\tilde{M}$ ,  $M_p$  and  $P$ , respectively. As the concentrations  $C_p^p$  and  $C_v^p$  are calculated on the centered grid, to solve (13) we use the upstream scheme.

### 3. 1D atmospheric simulation

#### 3.1. Simulation of the TOGA COARE case

For evaluation purpose, the one-dimensional version of the atmospheric model LMDz is applied to the TOGA COARE case (Ciesielski et al. 2003).

TOGA COARE is an international campaign which was conducted from 1 November 1992 to 28 February 1993 in the western Pacific warm pool centered at 2°S and 155°E. This region is associated with a warm sea surface temperature (during the four months the SST was 29.4°C on average). Within this period, two Madden-Julian oscillation (MJO) active phases occurred during the second half of December and during February (Chen et al. 1996; Yanai et al. 2000). Between 20 and 24 December, maximum convection developed and reached its peak on 24 December. These two phases are interspersed with a low convective activity period. During the experiment, the two MJO active phases in the Pacific Ocean are related to the presence of two convective clusters.

This atmospheric variability is particularly interesting to study the correlation of the tracer distribution with the convective activity. In the literature, observations of the campaign have been used to optimize Emanuel's convective scheme (Emanuel and Živković-Rothman 1999), to validate simulated isotopic compositions of water (Bony et al. 2008) or to model tracer transport using a cloud-resolving model (Salzmann et al. 2004).

We use a single column model whose physical parametrizations are close to that of Hourdin et al. (2006) except for an extension of the model to the stratosphere (Hourdin et al. 2012a,b): the vertical resolution is increased to 39 layers (the grid is stretched near the surface: first grid point at 35 m and 8 grid points in the first kilometer; mean resolution of 800 m between 1 and 20 km, and last point at 40 km). As the SCM is forced by TOGA COARE data sets throughout the four months, simulated precipitation is in close agreement with available observations, as shown for daily precipitation in Figure 2 (top). Transport and convective scavenging of aerosols are parameterized in the previous section. For simplicity, we do not consider the subtlety of droplet formation processes: all CCN are assumed activated:  $\alpha_a = 1$  and  $\beta_m = 1$ .

Removal of tracers in stratiform clouds and by large-scale precipitation are also included in the model and are based on the parameterization of Reddy and Boucher (2004) (hereinafter referred to as RB04) close to the formulation of Giorgi and Chameides (1986), but with some changes such that the description of the scavenging process follows more closely the large-scale condensation parametrization. This scheme does not differentiate ice nucleation from water nucleation. More explanations of this scheme can be found in the appendix.

Tracer vertical advection is calculated from the forced vertical velocity. Horizontal advection is supposed to bring air of the same composition as the grid-cell air (horizontal winds cannot sweep away radionuclides from the region.)

#### 3.2. Radionuclide tracer

As its source is mainly located in the upper troposphere and above,  $^{7}\text{Be}$  is an appropriate tracer for parameterization assessment purpose and for emphasizing the role of precipitation and of convective downdrafts.

$^{7}\text{Be}$  is a natural radionuclide (half-life of 53.3 days) and a useful tracer of the short-term atmospheric processes. It has a global continuous well-known source and is naturally produced by spallation reactions induced by high energy cosmic ray protons and neutrons on nitrogen and oxygen in the stratosphere and upper troposphere (Lal and Peters 1967, hereinafter LP67). After its production,  $^{7}\text{Be}$  attaches indiscriminately to ambient submicrometric aerosols (Bondietti et al. 1987) and is transported by them.  $^{7}\text{Be}$  is chemically nonreactive and may be considered as a passive tracer. It is removed by radioactive decay and by wet and dry deposition, although the dominating removal process is scavenging by convective and large-scale precipitation. Thus the mean residence times in the troposphere is ranging from 10 to 35 days (Shapiro and Forbes-Resha 1976; Bleichrodt 1978; Koch et al. 1996; Liu et al. 2001). Despite the different temporal variabilities of this radionuclide concentration, reported in LP67 and Koch and Mann (1996), interannual  $^{7}\text{Be}$  surface concentration variability is negligible as reported by Yoshimori (2005).

In our model, the source of the radionuclide is an adaptation of LP67 with constant concentrations depending on the latitude and the model layers but not on the solar activity. The initial tracer profile is taken from a previous GCM simulation (Heinrich and Jamelot 2011) at 2°S and 155°E, location of the TOGA COARE.

#### 3.3. Results

The numerical experiments have been performed over the period of four months. We focus on two different periods showing the alternation between active and suppressed phases of the MJO which are characterized by high and low convective intensity, respectively.

As described by Yanai et al. (2000), a first cloud cluster reached the experiment site in mid-December and was accompanied by heavy rainfalls as shown in

Figure 2. Convection slowed down around 25 December and diminished early January. Then the cluster drifted farther west and disappeared near  $170^{\circ}$  W around 10 January. The next period is associated with the MJO suppressed phase, and is characterized by moderate precipitation. Finally, a second cluster reached the site in early February, resulting in intense convection during this month but in less precipitation than in December. The staged convective development associated to the MJO is well detailed in Kikuchi and Takayabu (2004).

The analysis of MJO periods by Chen et al. (1996), confirmed by the convection analysis in our simulations leads us to define the two periods as follows: from 20 December 1992 to 5 January 1993 for the active phase, from the 6 January to 26 January 1993 for the suppressed phase.

In order to study the contribution of convective scavenging in comparison to that of stratiform scavenging, and interaction of both convective and stratiform clouds on tracer distribution, two simulations are made without and with convective scavenging, hereafter referred to as simulations A and B, respectively. Another simulation is made without scavenging by stratiform precipitation and clouds (simulation C) in order to single out the role of convective transport. All the simulations are made on the whole TOGA COARE experiment.

The three simulations are detailed in Table 1. All simulations take into account removal of radionuclide tracers by radioactive decay, by dry deposition (dry deposition flux to the ground is assumed to be proportional to the aerosols concentration in the lowest model layer and to a velocity set to  $0.1 \text{ cm s}^{-1}$ ), and transport by convective drafts.

The simulations are illustrated in Figure 2 showing the  $^{7}\text{Be}$  concentration time series simulated for the two periods. Simulated concentrations in Figure 2 show large temporal variations from the surface to the top of the troposphere, and large differences between the three simulations in the whole troposphere. This highlights a strong cleansing by large-scale clouds and associated precipitation. Thereafter, only simulation B is studied in detail, but the vertical profile of the tracer is compared with the two other simulations.

Table 1. Simulations and model parameters used in the simulations

Simulation	Convective clouds	Stratiform clouds
A	transport by air	in-cloud scavenging, impaction by rain
B	transport by air, in-cloud scavenging, impaction by rain	in-cloud scavenging, impaction by rain
C	transport by air, in-cloud scavenging, impaction by rain	NONE

The analysis of these results is based on:

1. The comparison of the vertical distributions of simulated precipitation fluxes between the two periods (Figure 3).

2. The comparison of tracer concentrations between the simulations A and B (Figures 4a, 5a, right) and of

tracer tendencies (Figures 4a, 5a, left) for each period. Convective tracer tendencies in the saturated drafts and in the unsaturated downdraft are represented separately. Both include the effect of precipitation and their sum is equal to the total convective tendency as defined in Eq. (1). Over the entire troposphere the tendency induced due to convective saturated drafts is owing almost entirely to the last two terms of Eq. (10a), viz the compensating subsidence and the scavenging terms (not shown). Large-scale tendency is separated into nucleation and impaction tendencies. Effect of large-scale precipitation evaporation is the difference between the total tendency and nucleation and impaction tendencies.

3. The comparison of the convective mass fluxes between the two periods (Figures 4b, 5b). The analysis is focused on the effect of both convection and large-scale precipitation on the tracer distribution. The contribution of other processes is not discussed.

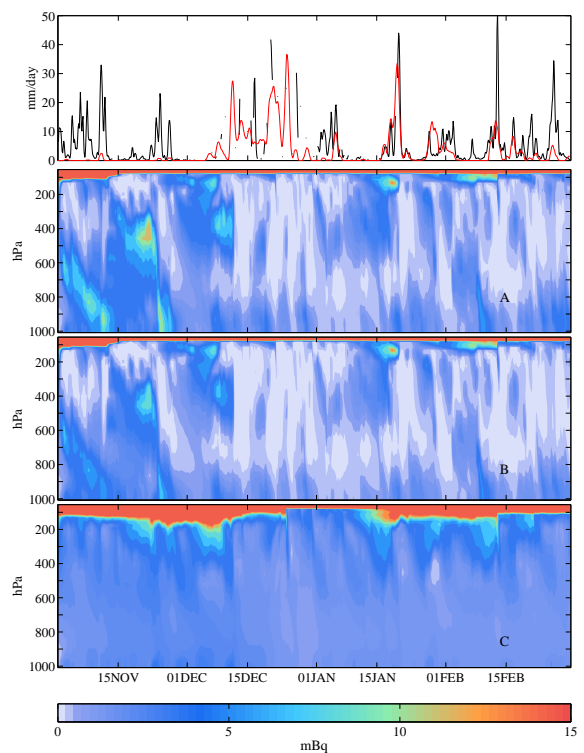


**Figure 2. Top panel:** Observed surface precipitation (black line) and simulated stratiform precipitation (red line) ( $\text{mm day}^{-1}$ ) over the four months of TOGA COARE. Considering how the forcing in the SCM is made, the simulated surface precipitation is consistent with the observed one and the difference between red and black lines gives approximatively the convective precipitation.

**Lower panels:**  $^{7}\text{Be}$  concentrations ( $\text{mBq kg}^{-1}$ ) simulated by LMDz SCM in the simulations A, B and C (see table 1). Above  $33 \text{ mBq kg}^{-1}$  details on concentrations are not shown for concentrations of lower atmosphere to be displayed.

Convection intensity is closely related to precipitation fluxes as shown in Figure 3, where the suppressed phase, in the absence of a cluster, is characterized by low values of these fluxes from the surface to the top of the troposphere, which is located around 18 km. The vertical precipitation flux gradient is also an indicator of precipitation behavior. A positive vertical gradient is associated with the evaporation of rain, which is

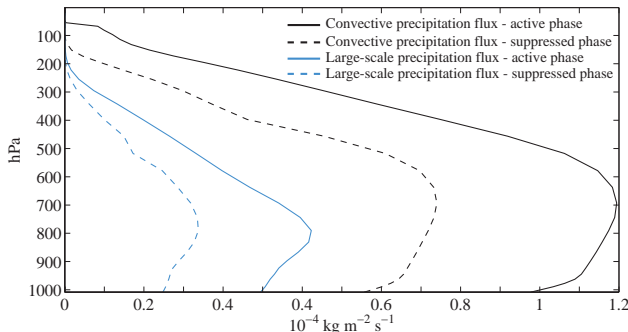


**Figure 3.** Simulated vertical profiles of convective (black) and large-scale (blue) precipitation flux ( $10^{-4} \text{ kg m}^{-2} \text{ s}^{-1}$ ) during the active phase (solid line) and the suppressed phase (dashed line).

likely to release tracers. For both phases, this positive gradient is the largest between the surface and 950 hPa.

### 3.3.1. Active phase

The active phase is characterized by heavy rainfalls (Figures 2 and 3) and large convective fluxes (Figure 4b). The cloud top is located above 100 hPa, where all mass fluxes become negligible. Whilst tendencies induced by large-scale and convective clouds and precipitation are of the same order of magnitude, adding the convective scavenging leads only to a 20% to 30% decrease of  $^{7}\text{Be}$  concentration (Figure 4a, right). At the base of the atmosphere, tracer release by precipitation evaporation increases the concentration.

In the upper troposphere (between 50 and 500 hPa), both large-scale and convective total tendencies are negative: large-scale condensation of water removes by nucleation tracers from the environment while deep convection detrains at these levels low level air with low  $^{7}\text{Be}$  concentration. Large-scale clouds release tracer at lower levels by evaporation of their precipitation (mostly around 450 hPa) where the difference between the large-scale total tendency and the in-cloud large-scale scavenging tendency is largest.

Between 500 and 800 hPa, large-scale clouds still remove tracer by nucleation whereas deep convective processes tend to increase concentrations. The compensating subsidence (since the tendency induced by the saturated drafts is almost equal to the total convective tendency) explains most of the positive total convective tendency; it brings down high concentrations from the upper troposphere to altitudes where the concentrations are lower (Figure 4a, left).

Below 800 hPa, the conversion to precipitation is very weak in convective saturated drafts so that the convective tendency is only due to the effect of the compensating subsidence and of the unsaturated downdrafts. The vertical gradient of  $^{7}\text{Be}$  concentration is zero in the well mixed boundary layer (below 950 hPa) and negative above, and so is the tendency due to saturated drafts. The tendency due to the unsaturated downdraft is weak above cloud base (950 hPa) and large below where precipitation evaporates at a high rate and the mass flux of the downdraft is strongly diverging (Figure 4b). This tendency increases rapidly close to the surface, reaching values as high as  $0.03 \text{ mBq kg}^{-1} \text{ h}^{-1}$ .

Scavenging in large-scale clouds decreases from 800 hPa to 950 hPa where it reaches zero, but the decrease is not regular: precipitating clouds form between 900 hPa and 950 hPa. This cloud layer is associated with a minimum of relative humidity around 900 hPa (not shown), which yields the maximum evaporation of large-scale rain at 900 hPa.

Impaction by convective precipitation has little effect, regarding to the size of the aerosols to which  $^{7}\text{Be}$  are attached, the size of the raindrops in the model and the respective collision efficiency. Impaction scavenging by large-scale precipitation is very low (close to zero) compared to the other tendencies, although we use the same raindrop size as for the convective rain.

The mean wet deposit due to convective and large-scale precipitation is  $1739$  and  $7531 \text{ mBq m}^{-2} \text{ d}^{-1}$ , respectively.

### 3.3.2. Suppressed phase

This period with weaker convection is characterized by moderate precipitation (Figure 2) and smaller convective fluxes (Figure 5) compared to the active phase. Most of the above mentioned processes are present but are attenuated as illustrated in Figure 5. Scavenging of tracers occurs between the top cloud and 500 hPa (Figure 5a, left) and is caused mainly by nucleation in large-scale and convective clouds. Precipitation of the unsaturated downdraft also removes tracers from the environment.

Between 500 and 750 hPa, the compensating subsidence brings down rich concentrations, the tendency induced by the convection is positive. Below, between 750 and 900 hPa, compensating subsidence brings down poor concentrations, the tendency induced by the convection is thus negative. Below 800 hPa, tracers release by evaporation in the unsaturated downdraft and by evaporation of large-scale precipitation yields larger concentrations of tracers as shown on Figure 2 or in Figure 5a (left). At the surface, this process produces the positive peak of the tendency in the unsaturated downdraft (Figure 5a, left) and equals the positive tendency produced by the large-scale precipitation evaporation. Release of tracers by evaporation has also a larger effect, in this phase, than compensating subsidence.

Again impaction scavenging is negligible.

The mean wet deposit due to convective and large-scale precipitation is  $928$  and  $6226 \text{ mBq m}^{-2} \text{ d}^{-1}$ , respectively.

### 3.3.3. Relative significance of processes at the surface

Mean convective and large-scale tendencies on Figures 4 and 5 show that tracer distribution is dependent on convective transport and scavenging as well as scavenging by large-scale clouds and associated precipitation. In the PBL, both of the tendencies are positive (Figures 4 and 5) during active and suppressed phases, and of the order of magnitude  $0.5 \text{ mBq kg}^{-1} \text{ d}^{-1}$ , i.e.  $15 \text{ mBq kg}^{-1} \text{ month}^{-1}$ . In contrast, mean surface concentration stays below  $2 \text{ mBq kg}^{-1}$  (Figures 4a, 5a, right). This result from a balance between removal of tracer by entrainment into the saturated updraft, redistribution of PBL in upper layers of the

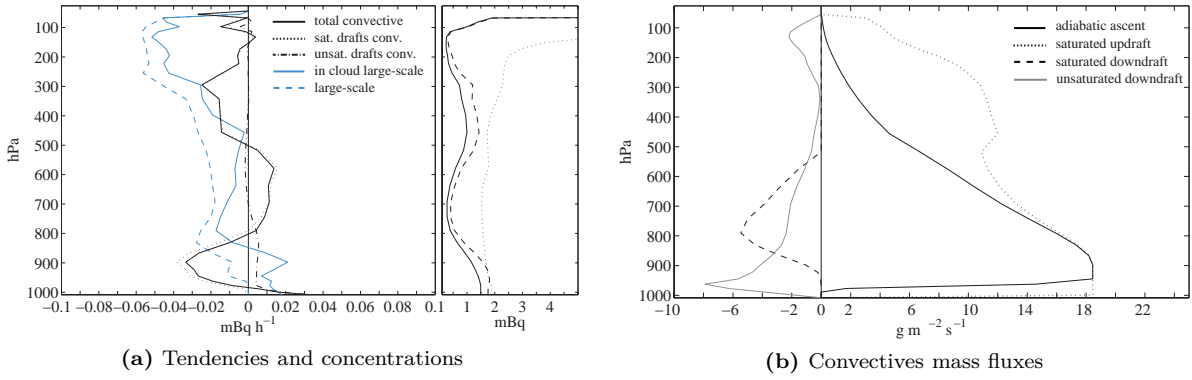


**Figure 4.** Active phase. (a) (left) Simulated vertical tendencies ( $\text{mBq kg}^{-1} \text{h}^{-1}$ ): total convective tendency of simulation B (solid black line) which is separated into two tendencies: saturated drafts with scavenging (black dotted line), unsaturated downdraft (black dashed line), total large-scale tendency (blue solid line) and in-cloud scavenging tendency (blue dashed line) (impaction scavenging is negligible and effect of evaporation is the difference between in-cloud scavenging and total tendencies); (right) the vertical profile of  ${}^7\text{Be}$  concentration ( $\text{mBq kg}^{-1}$ ) of the simulation A (dashed line), simulation B (solid line), simulation C (dotted line). (b) Simulated convective mass fluxes ( $\text{g m}^{-2} \text{s}^{-1}$ ): adiabatic ascent (solid black line), saturated downdraft (dashed line), saturated updraft (dotted line) and unsaturated downdraft (gray line).

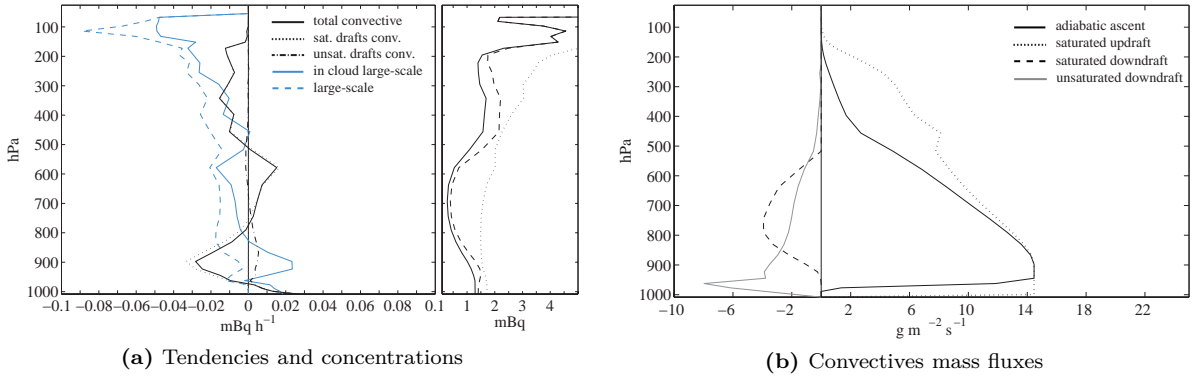


**Figure 5.** Suppressed phase during TOGA COARE. (a) same as Figure 4a and (b) same as Figure 4b.

troposphere and addition of tracers by evaporation of both convective and large-scale precipitation.

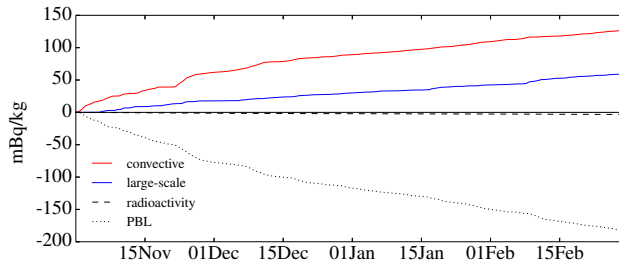


**Figure 6.** Cumulative tendencies in the first layer of the model (thickness  $z_1 = 70 \text{ m}$ ) induced by convection (red), large-scale precipitation (blue), boundary layer (dotted line) and radioactive decay (dashed line) in the TOGA COARE case (simulation B). The boundary layer tendency in the first model layer ( $(\partial_t C_1)_{\text{bl}}$ ) results from the balance between the dry deposit ( $\Phi_d$ ) and the turbulent flux at the layer top (parameterized as a vertical diffusion with eddy diffusivity  $K_z$ :  $\rho z_1 (\partial_t C_1)_{\text{bl}} = -\Phi_d + K_z (\partial_z C)(z_1)$ ).

Cumulative tendencies (Figure 6) underline the predominance of effects of deep convection on tracers

close to the surface during the whole experiment despite the alternation of MJO phases: convective tendency is larger by a factor of two compared to large-scale tendency. The tendency induced by processes occurring in the PBL (dotted line on Figure 6) is equal to the opposite of the sum of large-scale and convective tendencies (blue and red lines on Figure 6). Thus PBL balances effects induced by mechanisms associated with deep convection and large-scale clouds. It should be noted that, in the case where scavenging by convective processes are not active (simulation A), large-scale tendencies predominate over convective tendencies in the PBL.

The average wet deposit over the whole TOGA COARE period is 1392 and 4405  $\text{mBq m}^{-2} \text{d}^{-1}$  for the convective and large-scale precipitation, respectively.

### 3.3.4. Comparison with observations

Simulated  ${}^7\text{Be}$  surface concentrations are compared to daily averaged concentrations measured by a station located in Kavieng (150° E, 3° S), Papua New Guinea, close to the TOGA COARE Intensive Field Array. This station belongs to the International Monitoring

System (IMS), developed in the framework of the Comprehensive Test Ban Treaty. The station has been measuring airborne aerosols and particles with very low-level radioactivity (Schulze et al. 2000) since 2007. Measurements are erratic (there is no data during 2008, the first two months of 2010 and the second half of 2011). Nevertheless, as the interannual variability of  $^{7}\text{Be}$  surface concentration is of the order of the day to day variability, we compare simulations to interannual mean values and spread. Hence, Figure 7 presents the comparison between TOGA COARE simulations with observations available between 2007 and 2011 over the four months NDJF.

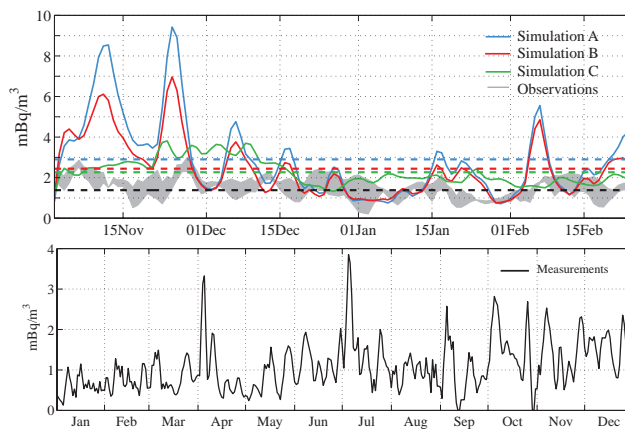


**Figure 7.** (top) Comparison of the daily simulated  $^{7}\text{Be}$  surface concentrations (blue: simulation A, red: simulation B and green: simulation C) and the CTBTO interannual minimum and maximum of the observations (the lower part of the shaded area corresponds to the minimum value of the data for each day, and the upper part corresponds to the maximum value) associated with their mean values in dashed lines over the 4 months of TOGA COARE.

(bottom) Surface concentrations of  $^{7}\text{Be}$  for 2007 measured at the IMS station located at  $150^{\circ}$  E,  $3^{\circ}$  S.

The main feature of deep convective transport associated with  $^{7}\text{Be}$  is to displace these tracers from upper troposphere and to bring them down to lower layers of the atmosphere. Moreover, concentrations within the PBL are enhanced as a result of tracers release by evaporation of convective and large-scale precipitations, the effect of the latter being dominant.

Mean values of simulated surface concentrations with convective scavenging ( $2.42 \text{ mBq m}^{-3}$ ) are lower than those simulated without convective scavenging ( $2.90 \text{ mBq m}^{-3}$ ), approaching the mean value of interannual observations ( $1.38 \text{ mBq m}^{-3}$ ). Mean simulated surface concentrations in simulation C, without scavenging by stratiform clouds and rain, ( $2.26 \text{ mBq m}^{-3}$ ) are the lowest ones. In simulation A, the absence of removal by convective precipitation is compensated for by a stronger wet removal by stratiform precipitation: stratiform precipitation, containing higher  $^{7}\text{Be}$  concentration, liberates more tracers when evaporating in the PBL than in simulation B.

Peaks in simulations A and B around the 10 and 25 November can be related to the large-scale nucleation in the upper troposphere as well as to the release in the lower layers by evaporation of the precipitation, which results in the downward transport of the tracer

to surface. These peaks are higher than the range of measured concentrations (Figure 7, bottom) and are, however, in the range of measured concentrations at other stations where MJO events occur (not shown here). It is worth to note that large-scale and convective scavenging can, by themselves, lead to a similar mean surface concentration and a similar variability (Figures 7: blue and green lines.) During the heavy rainfalls, the second half of December, large-scale precipitation cleans the troposphere and reduces surface concentrations.

As shown by the evident decrease of surface concentrations during the active phase (between the 12 December until the half of January) tracer are more scavenged when heavy rainfalls occur i.e. during MJO active phases. Conversely, during suppressed phases, light precipitation occurs and tracer concentration is higher.

#### 4. GCM simulations

In the GCM, subgrid-scale processes are solved for each column separately, making it possible to use the new parameterization (sections 2.1 and 2.2) in the three-dimensional model. The 3D approach has the advantage of being able to simulate the transport of terrestrial radionuclides such as  $^{210}\text{Pb}$ , which was not the case in the SCM owing to specific conditions at the surface.

The source of  $^{210}\text{Pb}$  atoms is the radioactive decay product of  $^{222}\text{Rn}$  which is emitted in the model from a soil reservoir 10 cm thick. The emission flux of  $^{222}\text{Rn}$  is prescribed to  $1 \text{ atom cm}^{-2} \text{ s}^{-1}$  on continents. Because of their respective lifetimes (3.8 days for  $^{222}\text{Rn}$  and 22 years for  $^{210}\text{Pb}$ ),  $^{210}\text{Pb}$  particles are continuously formed in the first layers of the model.

A two years climate simulation and a one year simulation with nudged horizontal winds have been performed in order to characterize the vertical distribution of the radionuclides and to compare with radionuclide observations from the IMS stations, respectively. Both simulations use the parameterization of section 2, the climate simulation uses the same parameters as in simulation B in section 3.

We use two parameterizations of large-scale scavenging. The first one (Genthon 1992) is identical to the one used in Heinrich and Jamelot (2011) and has been developed to study transport of dust and sea-salt aerosols over Antarctic. This scheme does not take into account release by evaporation of stratiform precipitation. We shall use it when comparing our simulations with the ones of Heinrich and Jamelot (2011) in order to assess the effect of the representation of convective scavenging. The second one, already used in the 1D simulations of the TOGA COARE case, follows more closely the physical processes represented in the GCM and will be used for climatological simulations.

The GCM simulations have been performed with a horizontal resolution of  $3.75^{\circ}$  in longitude and  $1.875^{\circ}$  in latitude. On the vertical, the model uses, as the SCM version, 39 levels.

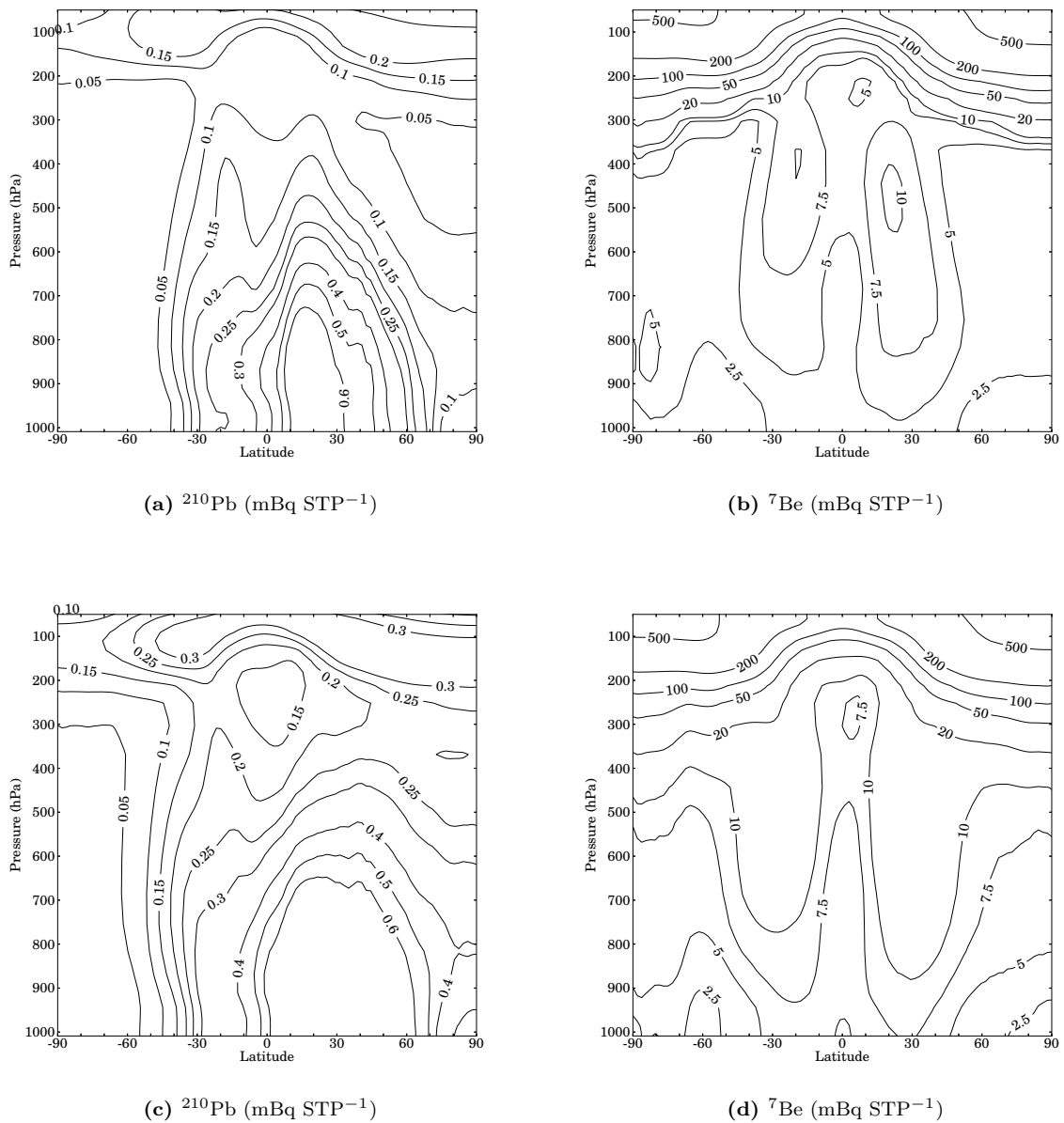


**Figure 8.** Zonal average of (a)  $^7\text{Be}$  and (b)  $^{210}\text{Pb}$  concentrations in mBq per unit of volume at the standard conditions for temperature and pressure (STP):  $1 \text{ mBq STP}^{-1} = 1.3 \text{ mBq kg}^{-1}$  approximately, using a fraction of the aerosols in the aqueous phase of large-scale clouds set to 70% as in Reddy and Boucher (2004) (see appendix for the various definitions of the aqueous phase). (c,d) Same as (a,b), except that the fraction of the aerosols in the aqueous phase of large-scale clouds is lowered to 10%.

#### 4.1. Climate simulations

##### 4.1.1. Vertical distribution

To characterize better the performance of the new scheme and to highlight the significant role of large-scale processes on tracer distribution, zonal mean of the concentrations of  $^{210}\text{Pb}$  and  $^7\text{Be}$ , averaged over the two years of climate simulations (1983 and 1984), is shown on Figure 8. Here the radionuclide concentrations are expressed in mBq per standard cubic meters to be comparable to the literature.

Figure 8 (a) shows, as reported by Giannakopoulos et al. (1999) and Liu et al. (2001), a minimum  $^{210}\text{Pb}$  concentration located in the upper tropical troposphere. Nucleation scavenging in deep convective

clouds causes this minimum and can be correlated with the  $^7\text{Be}$  minimum concentration (Figure 8 (b)). Over the southern mid-latitudes, values of  $^{210}\text{Pb}$  concentration are higher than those from Liu et al. (2001) and are attributed to large-scale nucleation scavenging that is likely less efficient in our model.

$^7\text{Be}$  concentrations emphasize the Hadley circulation with its dry descending branches over the Tropics.

Figures 8 (c,d) represent a simulation in which we have reduced the large-scale nucleation scavenging coefficient to 10%, compared to 70% (RB04) in order to decrease the effect of scavenging in large-scale clouds, particularly in the upper troposphere, as mentioned by Croft et al. (2010) and suggested by high surface concentration induced by this process in

the TOGA COARE case results (section 3.3.4). Since our model does not distinguish ice nucleation from liquid nucleation, the large-scale nucleation scavenging coefficient (given by  $\alpha$  in appendix A) is reduced to 10% for all clouds (whether liquid, ice or mixed). Assuming that large-scale nucleation scavenging is as inefficient in liquid clouds as in ice clouds is unphysical. For instance measurements by Henning et al. (2004) established that, for aerosols in the accumulation mode, the in-cloud scavenging coefficient is lower in ice and mixed phase clouds than in warmer clouds, i.e. lower than 0.2. While this approximation may affect quantitative results, we assume that it does not change significantly the main features of the radionuclide distributions. However, in this version of LMDz, low-level clouds are underestimated (Hourdin et al. 2006), thus the effect of this assumption is lightened for liquid clouds. The point is further discussed in the conclusion.

On Figures 8 (a,b) concentrations are lower than those of Liu et al. (2001) in the free troposphere and do not have the same patterns as in Liu et al. (2001). When scavenging by large-scale nucleation is reduced, general patterns are closer than in the study aforementioned. On Figure 8 (c), it is worth noting that  $^{210}\text{Pb}$  concentration is uniformly low over the southern high latitudes ( $< -50$  degrees) between the surface and 200 hPa. This is attributed to the scavenging associated with the large fraction of large-scale clouds present in the simulation at these latitudes (not shown).

Both of the radionuclide zonal distributions are consistent with simulations of Liu et al. (2001).

#### 4.1.2. Effect of the processes on the radionuclide distributions

Effects of deep convection and large-scale processes in the climate simulation, using a large-scale nucleation scavenging coefficient of 10%, are shown on Figure 9. Tendencies for the simulation with a large-scale nucleation scavenging coefficient of 70% are not shown: the spatial distribution of tendencies is quite similar but the tendencies have a different magnitude.

**$^{210}\text{Pb}$ :** While deep convection mainly impacts  $^{210}\text{Pb}$  concentrations in the Tropics (Figure 9 (a)), large-scale clouds affect its concentration mostly in mid-latitudes and at the lower altitudes, boundary layer included (Figure 9 (c)). Over Antarctica (Figure 9 (c)), tendencies are weak and negative (except for some positive tendency due to shallow convection), which is consistent with the very low concentrations in this region.

In the Tropics, all tendencies are negative above 300 hPa:  $^{210}\text{Pb}$  is brought above these levels by the ascending branch of the Hadley cells; there it is removed by both large-scale nucleation and convective scavenging. A part of the scavenged  $^{210}\text{Pb}$  is released between 300 and 500 hPa by evaporation of stratiform precipitation.

In the Tropics, convective tendencies are mainly negative (Figure 9 (a)) which means that all the  $^{210}\text{Pb}$  lifted in convective updrafts is removed by convective scavenging. Because the conversion into precipitation is very efficient in convective saturated drafts, most

of the entrained radionuclides are transferred into the convective precipitation. Convective precipitation evaporates in the low troposphere and releases the radionuclide between 900 and 975 hPa. However, convective tendency is negative close to the surface: owing to the compensating subsidence, this process brings down low concentration air at levels where the concentration is higher because of the terragenic source of  $^{210}\text{Pb}$ .

**$^7\text{Be}$ :** Figure 9 (b) shows that deep convection affects  $^7\text{Be}$  concentrations predominantly in the Tropics with a behaviour similar to that observed in the SCM simulation (Figures 5 and 4) but the magnitude of the tendencies in the climate simulations are approximately threefold larger. In the upper troposphere (between 200 and 500 hPa), deep convection detains at these levels low level air with low  $^7\text{Be}$  concentrations. Below 500 hPa, the conversion to precipitation is very weak in convective saturated drafts so that the convective tendency is only due to the effects of the compensating subsidence and of the unsaturated downdrafts. Except in the PBL, in which tracers are released by evaporation of convective precipitation, the vertical gradient of  $^7\text{Be}$  concentration is affected by large-scale processes as shown by the Figure 9 (d).

Large-scale nucleation at high altitudes (between 50 to 400 hPa in the mid-latitudes and between 50 to 250 hPa in the Tropics) removes  $^7\text{Be}$  radionuclide (Figure 9 (d)). Below these altitudes, nucleation scavenging alternates successively with release by evaporation of stratiform precipitation.

Between 900 hPa and the surface, the large-scale tendency is essentially due to the release of tracers by evaporation of precipitation.

#### 4.1.3. Budgets

Annual global budgets of  $^7\text{Be}$  and  $^{210}\text{Pb}$  in climate simulations are given in table 2. The tropopause is defined using the criterion of  $2^\circ\text{C km}^{-1}$  lapse rate as defined by the World Meteorological Organization.

Table 2. Annual average global budgets and residence times of tropospheric  $^7\text{Be}$  and  $^{210}\text{Pb}$  in climate simulations for two large-scale in-cloud scavenging coefficients.

Fraction of activated CCN	$^{210}\text{Pb}$		$^7\text{Be}$	
	0.7	0.1	0.7	0.1
Source ( $\text{g d}^{-1}$ )	37	37	0.25	0.22
from stratosphere	—	—	0.08	0.05
within troposphere	37	37	0.17	0.17
Burden (g)	244	389	2.3	3.7
Sinks ( $\text{g d}^{-1}$ )	37.4	37.1	0.25	0.22
wet deposition				
- convective	10.4	15.6	0.04	0.06
- stratiform	27	21.5	0.17	0.11
dry deposition	$10^{-5}$	$10^{-5}$	0.01	0.02
radioactive decay	0.05	0.03	0.03	0.03
Residence time (d)	6.5	10.5	9.2	16.8

Contrary to Liu et al. (2001)'s study, in our model the wet deposition is predominantly induced by large-scale processes. As expected, when reducing the fraction of aerosols on the aqueous phase in

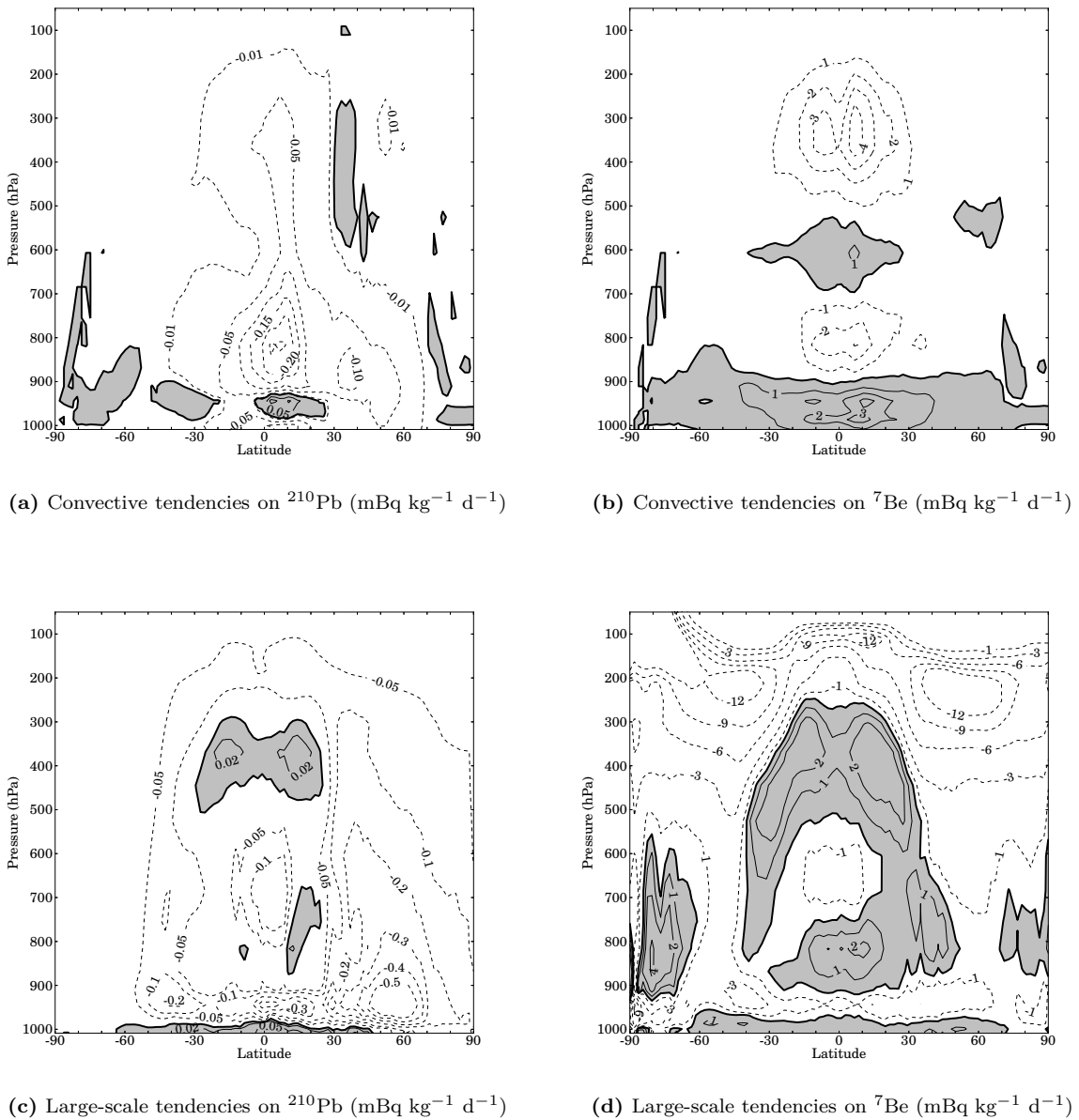


**Figure 9.** Simulated vertical tendencies on  $^{210}\text{Pb}$  and  $^7\text{Be}$  ( $\text{mBq kg}^{-1} \text{d}^{-1}$ ), in the climate simulation: (a,b) induced by convection and (c,d) by large-scale processes. The thick line represents  $0 \text{ mBq kg}^{-1} \text{d}^{-1}$  and gray areas correspond to positive tendencies.

large-scale clouds, the convective scavenging increases, thus balancing partly the decrease of the large-scale scavenging.

Residence times of  $^7\text{Be}$  in the troposphere are 9.2 days in the standard simulation (the fraction of aerosols on the aqueous phase in large-scale clouds is 0.7) and 16.8 days when this fraction is reduced to 0.1. Reducing nucleation scavenging in large-scale clouds improves the  $^7\text{Be}$  residence time which is in the range of the values from the literature: from 10 to 35 days (Shapiro and Forbes-Resha 1976; Bleichrodt 1978; Koch et al. 1996). Residence times of  $^{210}\text{Pb}$  are 6.5 and 10.5 days for the standard simulation and for the one with the reduced fraction of activated CCN, respectively. In both simulations,  $^{210}\text{Pb}$  residence times are in the range of the ones from the literature.

#### 4.2. Nudged GCM simulations

##### 4.2.1. Evaluation with surface measurements

The GCM has been simulated over the 2007 year. Concentrations have been initialized from those calculated by a three months simulation, to avoid underestimation of concentrations compared to measurements during the first months of the 2007 year. GCM horizontal winds are nudged toward analyzed 6 hourly time wind fields of the European Centre for Medium-Range Weather Forecasts (ERA-Interim). As in the SCM study, simulations are performed turning on or off convective scavenging and results are compared with observations. Unlike SCM simulations, we use the large-scale scavenging parameterization of Genton (1992), inspired by the

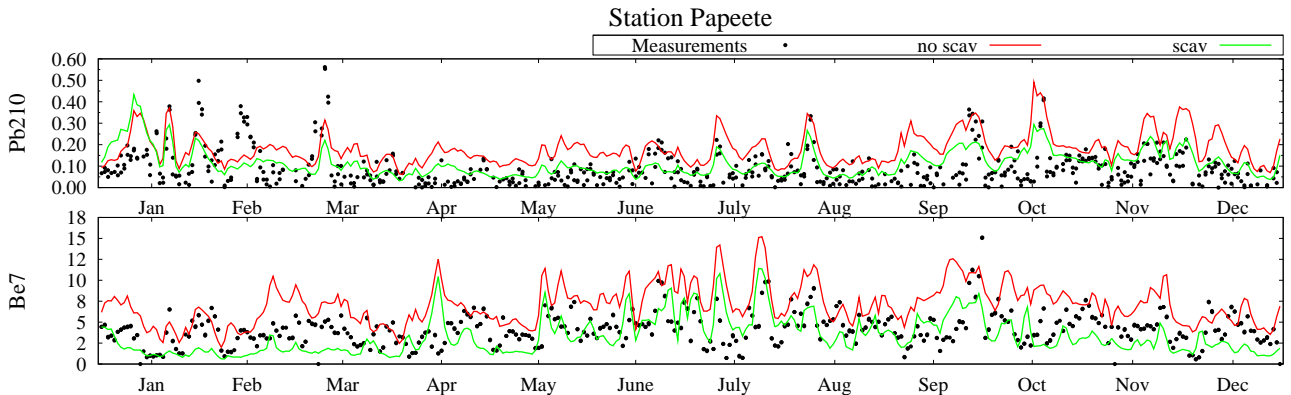


**Figure 10.** Time series for the year 2007 of daily measured concentrations (dots) and simulated daily concentrations in  $\text{mBq m}^{-3}$  of  $^{210}\text{Pb}$  and  $^7\text{Be}$  (red line: without convective scavenging, green: with convective scavenging) at Tahiti station.

one of Radke et al. (1980), in which nucleation and impaction scavenging is calculated by integrating the quantity of tracer scavenged by either condensation or precipitation impaction. Release by evaporation of large-scale precipitation is not taken into account. Results and discussion of this simulation is illustrated on Figures 10 and 11 and applies only for these figures.

The goal here is not to validate or to calibrate the new parameterization but rather to test it at a global scale and particularly in tropical regions. Surface concentrations in the tropics are illustrated (Figure 10) by daily averaged concentrations of  $^{210}\text{Pb}$  and  $^7\text{Be}$  at the IMS station of Tahiti (French Polynesia), which presents a nearly full set of observations during the 2007 year.

As expected for stations located outside the Inter Tropical Convergence Zone (ITCZ), the main effect of convective scavenging is to decrease concentrations of both radionuclides all over the year. In the absence of this process (red line on Figure 10), the yearly averaged concentrations of  $^{210}\text{Pb}$  and  $^7\text{Be}$  ( $0.18$  and  $7 \text{ mBq m}^{-3}$ , respectively) are largely overestimated compared to observations ( $0.06$  and  $4 \text{ mBq m}^{-3}$ ). The new parameterization reduces concentrations of  $^{210}\text{Pb}$  and  $^7\text{Be}$  to  $0.10$  and  $5 \text{ mBq m}^{-3}$ , respectively, which are close to results of Heinrich and Jamelot (2011). Contrary to the TOGA COARE case, aerosol release by evaporation of convective precipitation is not dominant at this station, as confirmed by the analysis of tracer tendencies. Maps of concentrations (not shown) emphasize the major role of evaporation within ITCZ which yields high peaks of  $^7\text{Be}$  during intense convective periods.

#### 4.2.2. Tracers in precipitation

Several studies have investigated concentrations of  $^7\text{Be}$  in precipitation. Ayub et al. (2009) have measured  $^7\text{Be}$  content in precipitation in central Argentina, at a semi-arid and subtropical region. They measured an annual concentration around  $1.7 \text{ Bq L}^{-1}$ , i.e.  $10^4 \text{ atoms g}^{-1}$ , with summer and winter  $^7\text{Be}$  concentrations in precipitation around  $2 \text{ Bq L}^{-1}$  ( $1.2 \cdot 10^4 \text{ atoms g}^{-1}$ ) and around  $1 \text{ Bq L}^{-1}$  ( $0.6 \cdot 10^4 \text{ atoms g}^{-1}$ ), respectively. The model reproduces a similar annual

concentration in central Argentina ( $10^4 \text{ atoms g}^{-1}$ ), although the seasonal cycle of  $^7\text{Be}$  concentrations in precipitation are the opposite of the observations ( $0.9 \cdot 10^4$  and  $2 \cdot 10^4 \text{ atoms g}^{-1}$  for summer and winter concentration, respectively). It is explained by rare and mainly stratiform winter precipitation, and by summer precipitation, which is entirely convective at this location.

Kadko and Prospero (2011) have measured  $^7\text{Be}$  concentrations in precipitation in the Bermudas and found an annual concentration of  $1.2 \cdot 10^4 \pm 0.5 \cdot 10^4 \text{ atoms g}^{-1}$ . In LMDz, at this location, the value is  $0.9 \cdot 10^4 \text{ atoms g}^{-1}$ , which is in the range of the observations.

$^7\text{Be}$  concentration in precipitation have also been measured by Heikkilä et al. (2008) over Switzerland. Simulated  $^7\text{Be}$  monthly concentration in precipitation at those locations are compared to observations and are shown on Figure 11. The mean value of the observations at Jungfraujoch and Dübendorf are  $8200$  and  $12200 \text{ atoms g}^{-1}$ , respectively which is in the range of what Ayub et al. (2009) and Kadko and Prospero (2011) measured at different locations.

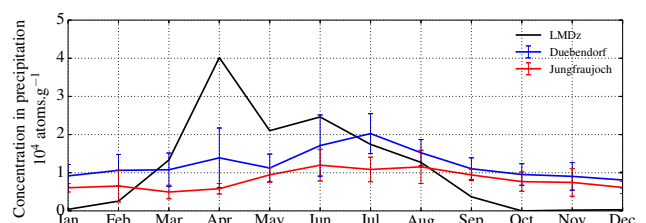


**Figure 11.** Concentration in precipitation of  $^7\text{Be}$  measured by Heikkilä et al. (2008), averaged over eight years (1998–2005), at Jungfraujoch (blue) and at Dübendorf (red) in Switzerland, and simulated concentration (black) in convective precipitation for 2007 at the same location (owing to the LMDz GCM resolution, both of the locations are in the same grid cell).

Heikkilä et al. (2008) conclude that the seasonality of the measured radionuclide is similar to the precipitation rate, which allows us to compare the concentrations of  $^7\text{Be}$  with their measurements. Owing to the duration of the three-dimensional simulation, we look at the  $^7\text{Be}$  concentrations in precipitation of the

nudged simulation at the same location in Switzerland. Simulated concentrations are shown on Figure 11.

The annual cycle is well captured despite the fact that the large-scale scavenging parameterization (Genthon 1992) used in the simulation does not provide the tracer concentration in large-scale precipitation. Concentrations are larger and of the same order of magnitude during summertime. Concentrations are low (almost zero) during wintertime. The large amount of tracer in precipitation during summer is correlated with the simulated precipitation (not shown here) which is mostly convective during this period. Furthermore, the concentration peak in April is correlated with a high  $^7\text{Be}$  concentration owing to low tropopause. Hence, convective clouds displaced through precipitation high  $^7\text{Be}$  concentrations to the surface.

## 5. Conclusions

A new parameterization of aerosol scavenging has been implemented in Emanuel's deep convective scheme. It makes it possible to analyze separately the effects of various components of the convective process onto the concentration of tracers attached to aerosols: the transport in the convective drafts, the scavenging in the saturated drafts, the redistribution of aerosols by detrainment and by precipitation evaporation and the elimination of aerosols by precipitation. Transport and scavenging have been evaluated using the single-column version of the LMDZ GCM in simulations of the four months long TOGA COARE case over ocean. Thanks to its high troposphere origin and its lifetime (53 days) longer than the studied processes,  $^7\text{Be}$  is an ideal tracer for investigating the mechanisms which move aerosols downwards: precipitation processes, convective compensating subsidence and convective unsaturated downdrafts. Without these processes, concentrations of  $^7\text{Be}$  in the troposphere and particularly at the surface should be lower than a few  $\text{mBq m}^{-3}$ .

The simulated mean concentrations of  $^7\text{Be}$  are of the same order of magnitude as those of the observations over the four month period, which allows their use for better understanding of the respective roles of processes responsible for the vertical distribution of  $^7\text{Be}$ .

It appears that the effect of large-scale cloud formation and related precipitation processes interacts strongly with the effect of deep convection processes. SCM results indicate that in-cloud scavenging, both by convective and large-scale processes, plays a significant role on high tropospheric tracer distribution, with a strong negative tendency. On the contrary, below-cloud evaporation plays a significant role on surface concentration with a strong positive tendency. The compensating subsidence of deep convection, by bringing down air rich in  $^7\text{Be}$ , has a positive effect on tracer concentration in the mid-troposphere. Large-scale clouds also move down tracers after successive nucleation and evaporation of precipitation. Convective impaction has a minor impact on environmental tracers and impaction from large-scale precipitation is negligible for these simulations.

Overall, large-scale nucleation scavenging appears to be more efficient to clean the atmosphere than moist convection. Large-scale scavenging has a major influence on aerosol cleansing in the troposphere,

especially in the upper troposphere; tracer release by evaporation of convective precipitation dominates in the PBL. Zonal and vertical distributions of  $^7\text{Be}$  and  $^{210}\text{Pb}$  indicate the significance of large-scale nucleation in the tracer distribution. Reducing the efficiency of large-scale nucleation improves zonal and vertical distributions of  $^7\text{Be}$  and  $^{210}\text{Pb}$  in our simulations. However, large-scale removal processes still need to be studied since, in our model, the large-scale nucleation does not differentiate ice nucleation from water nucleation, which is not consistent with the formulation of large-scale precipitation in LMDZ. This last result could arise from compensating errors from both the scavenging schemes and the large-scale clouds and precipitation scheme, as well as from the model underestimation of low-level clouds. It is also possible that in LMDz large-scale clouds and precipitation are too dominant and replace convection. At any rate, the first improvement of the model in future simulations will be to introduce a phase dependence for the large-scale nucleation coefficient.

The study only focused on oceanic moist convection. Continental convection displays deeper and more intense updrafts. Moreover it is expected to yield stronger low level evaporation. Both features should make the role of deep convection more prominent over land than over ocean.

As 3D GCM simulations are likely to represent better the intricacy of tropical convective systems, the new scheme has been also introduced and tested in the atmospheric general circulation model LMDz, using two natural radionuclides,  $^{210}\text{Pb}$  and  $^7\text{Be}$ . Due to their opposite sources, this couple of radionuclides should provide constraints on the parameterization of convective scavenging. Preliminary results encourage us to carry on the validation and calibration of this parameterization in the GCM.

## A. Parameterizations of the large-scale scavenging

*The original Preiss and Genthon parameterization*

Genthon (1992) defined a wet deposition model for stratiform precipitation, based on the model of Giorgi and Chameides (1986), but expressed the large-scale nucleation and impaction scavenging coefficients differently.

If  $\tilde{C}$  is the mass concentration of the tracer, its variation  $\delta_t \tilde{C}$  over a time increment  $\delta t$  reads:

$$\delta_t \tilde{C} = \lambda_{LS} \tilde{C}, \quad (\text{A.1})$$

with  $\lambda_{LS} = (1 - e^{-\eta Q})$  the scavenging coefficient and  $Q = P \delta t$ , where  $P$  (in  $\text{kg m}^{-2} \text{s}^{-1}$ ) is the precipitation flux (calculated at each level of the model) and  $\eta$  is a coefficient expressed in  $\text{m}^2 \text{kg}^{-1}$ . According to Radke et al. (1980),  $\eta$  depends on the scavenging (nucleation or impaction) and on the precipitation (liquid or solid).

Preiss and Genthon (1997) suggest that the coefficient  $\eta$  should be much weaker for impaction than for nucleation scavenging and test the values 1 and 0 for nucleation and impaction scavenging. In our simulations, we do not distinguish between solid and liquid precipitation and set  $\eta$  to 0.75 and  $0.5 \text{ m}^2 \text{ kg}^{-1}$  for nucleation and impaction scavenging, respectively.

**In-cloud scavenging** is assumed equal to  $\beta f \alpha$ , within each model layer, where  $f$  is the cloud fraction defined by Le Treut and Li (1991),  $\alpha$  is the fraction of tracer in the aqueous phase (set to 0.7 in RB04) and  $\beta$  is the rate of conversion of cloud water to rain water. If  $S_P$  is the amount of precipitation formed per unit mass of air and  $q_l$  the amount of condensed water per unit mass of air, then  $\beta = S_P/q_l$ . In order to compute  $\beta$ , RB04 estimate  $S_P$  from the precipitation divergence while the amount of condensed water is determined from the cloud cover and a prescribed in-cloud water content  $q_{l0}$  (set to 0.5 g kg<sup>-1</sup>):  $q_l = f q_{l0}$ . In our modified version, we follow more closely the large-scale condensation parameterization: we compute directly  $\beta$  within this parameterization, where  $q_l$  and  $S_P$  are available at every time-step, every level, every grid cell.

**Impaction** is dealt with in a fashion similar to the impaction by convective precipitation (subsection 2.5), although the precipitation is not correlated to any precipitation fraction, in accordance with Reddy and Boucher (2004). In each grid point, impaction scavenging is parameterized by integrating the volume swept by falling raindrops in the layer  $k$ :

$$(\partial_t \tilde{C})_{imp, LS} = -\Lambda_{LS} \tilde{C}_k. \quad (\text{A.2})$$

The scavenging coefficient  $\Lambda_{LS}$  reads:

$$\Lambda_{LS} = \mathcal{E}_{LS} \frac{3(P_k + P_{k+1})/2}{4 \rho_l r}, \quad (\text{A.3})$$

where  $\mathcal{E}_{LS}$  is the impaction efficiency set to  $10^{-3}$  and  $10^{-2}$  for raindrops and snowflakes, respectively, based on measurements compiled by Pruppacher and Klett (1996), and  $r$  the mean raindrop radius (set to 1 mm by Reddy and Boucher (2004)).

**Release by evaporation:** The concentration of tracer in the precipitation evaporated within a given layer  $k$  is assumed to be a fraction  $\nu$  (set to 0.5 in RB04) of the concentration of tracer in the precipitation. RB04 and our modified version differ in the concentration used to compute this fraction: in RB04 it is the concentration  $C_{p,k+1}$  in the precipitation entering the layer, while in our version it is the concentration  $C_{p,k}$  in the precipitation within the layer  $k$ . Thus, in our version, the amount  $E_k$  of tracer released by evaporation within the layer  $k$  reads  $E_k = \nu(P_{k+1} - P_k)C_{p,k}$  (where  $P_{k+1}$  and  $P_k$  are the precipitation fluxes at upper and lower interfaces of layer  $k$ ). Then, from tracer conservation, an expression of  $E_k$  in terms of  $P_{k+1}$  and  $C_{p,k+1}$  follows:

$$E_k = P_{k+1}C_{p,k+1} \frac{\nu \gamma}{1 - \gamma(1 - \nu)} \quad (\text{A.4})$$

where  $\gamma = (P_{k+1} - P_k)/P_{k+1}$ . With this equation the case of complete evaporation is not a special case since  $E_k \rightarrow P_{k+1}C_{p,k+1}$  when  $\gamma \rightarrow 1$ . On the contrary, RB04 (but also Liu et al. (2001)) have to treat this case separately.

## References

- Andreae, M., and Rosenfeld, D. (2008). Aerosol-cloud-precipitation interactions. part 1. the nature and sources of cloud-active aerosols. *Earth-Science Reviews*, 89, 13–41.
- Ayub, J. J., Gregorio, D. D., Velasco, H., Huck, H., Rizzotto, M., and Lohaiza, F. (2009). Short-term seasonal variability in <sup>7</sup>Be wet deposition in a semiarid ecosystem of central argentina. *Journal of Environmental Radioactivity*, 100, 977 – 981.
- Balkanski, Y. J., Jacob, D. J., Gardner, G., Graustein, W. C., and Turekian, K. K. (1993). Transport and residence times of tropospheric aerosols inferred from a global three-dimensional simulation of <sup>210</sup>Pb. *J. Geophys. Res.*, 98(D11), 20,573–20,586.
- Bleichrodt, J. (1978). Mean tropospheric residence time of cosmic-ray-produced beryllium 7 at north temperate latitudes. *J. Geophys. Res.*, 83, 3058–3062.
- Bondietti, E., Brantley, J., and Rangarajan, C. (1987). Size distributions and growth of natural and Chernobyl-derived submicron aerosols in tennessee. *Journal of Environmental Radioactivity*, 6, 99 – 120.
- Bony, S., and Emanuel, K. (2001). A parameterization of the cloudiness associated with cumulus convection; evaluation using TOGA COARE data. *J. Atmos. Sci.*, 58, 3158–3183.
- Bony, S., Risi, C., and Vimeux, F. (2008). Influence of convective processes on the isotopic composition ( $\delta^{18}\text{O}$  and  $\delta\text{D}$ ) of precipitation and water vapor in the tropics: 1. Radiative-convective equilibrium and Tropical Ocean-Global Atmosphere-Coupled Ocean-Atmosphere response experiment (TOGA-COARE) simulations. *J. Geophys Res.*, 113, D19305.
- Chen, S. S., Jr., R. A. H., and Mapes, B. E. (1996). Multiscale variability of deep convection in relation to large-scale circulation in TOGA COARE. *J. Atmos. Sci.*, 53, 1380–1409.
- Ciesielski, P. E., Johnson, R. H., Haertel, P. T., and Wang, J. (2003). Corrected TOGA COARE Sounding Humidity Data: Impact on Diagnosed Properties of Convection and Climate over the Warm Pool. *Journal of Climate*, 16, 2370–2384.
- Croft, B., Lohmann, U., Martin, R. V., Stier, P., Wurzler, S., Feichter, J., Hoose, C., Heikkilä, U., van Donkelaar, A., and Ferrachat, S. (2010). Influences of in-cloud aerosol scavenging parameterizations on aerosol concentrations and wet deposition in ECHAM5-HAM. *Atmospheric Chemistry and Physics*, 10, 1511–1543.
- Emanuel, K. (1991). A scheme for representing cumulus convection in large scale models. *J. Atmos. Sci.*, 48, 2313–2329.
- Emanuel, K., and Živković-Rothman, M. (1999). Development and evaluation of a convection scheme for use in climate models. *J. Atmos. Sci.*, 56, 1766–1782.
- Genthon, C. (1992). Simulations of desert dust and sea-salt aerosols in antartica with a general circulation model of the atmosphere. *Tellus*, 44B, 371–389.
- Giannakopoulos, C., Chipperfield, M. P., Law, K. S., and Pyle, J. A. (1999). Validation and intercomparison of wet and dry deposition schemes using <sup>210</sup>Pb in a global three-dimensional off-line chemical transport model. *Journal of Geophysical Research: Atmospheres*, 104, 23761–23784.
- Giorgi, F., and Chameides, L. W. (1986). Rainout lifetimes of highly soluble aerosols and gases as inferred from simulations with a general circulation model. *J. Geophys. Res.*, 91, 14,367–14,376.
- Greenfield, S. M. (1957). Rain scavenging of radioactive particulate matter from the atmosphere. *J. Meteor.*, 14, 115–125.
- Heikkilä, U., Beer, J., and Altimov, V. (2008). Beryllium-10 and beryllium-7 in precipitation in dübendorf (440 m) and at jungfraujoch (3580 m), switzerland (1998–2005). *J. Geophys. Res.*, 113.
- Heinrich, P., and Jamelot, A. (2011). Atmospheric transport simulation of <sup>210</sup>Pb and <sup>7</sup>Be by the LMDz general circulation model and sensitivity to convection and scavenging parameterization. *Atmospheric Research*, 101, 54–66.
- Henning, S., Bojinski, S., Diehl, K., Ghan, S., Nyeki, S., Weingartner, E., Wurzler, S., and Baltensperger, U. (2004). Aerosol partitioning in natural mixed-phase clouds. *Geophysical Research Letters*, 31.
- Hourdin, F., Foujols, M.-A., Codron, F., Guemas, V., Dufresne, J.-L., Bony, S., Denvil, S., Guez, L., Lott, F., Ghattas,

- J., Braconnot, P., Marti, O., Meurdesoif, Y., and Bopp, L. (2012a). Climate and sensitivity of the IPSL-CM5A coupled model: impact of the LMDZ atmospheric grid configuration. *Climate Dynamics, special issue.*
- Hourdin, F., Grandpeix, J.-Y., Rio, C., Bony, S., Jam, A., Cheruy, F., Rochetin, N., Fairhead, L., Idelkadi, A., Musat, I., Dufresne, J.-L., Lahellec, A., Lefebvre, M.-P., and Roehrig, R. (2012b). LMDZ5B: the atmospheric component of the IPSL climate model with revisited parameterizations for clouds and convection. *Climate Dynamics, (pp. 1–30).*
- Hourdin, F., Musat, I., Bony, S., Braconnot, P., Codron, F., Dufresne, J.-L., Fairhead, L., Filiberti, M.-A., Friedlingstein, P., Grandpeix, J.-Y., Krinner, G., LeVan, P., Li, Z.-X., and Lott, F. (2006). The LMDZ4 general circulation model: climate performance and sensitivity to parametrized physics with emphasis on tropical convection. *Climate Dynamics, 27, 787–813.*
- Jacob, D. (2000). Heterogeneous chemistry and tropospheric ozone. *Atmospheric Environment, 34.*
- Kadko, D., and Prospero, J. (2011). Deposition of  $^{7}\text{Be}$  to bermuda and the regional ocean: Environmental factors affecting estimates of atmospheric flux to the ocean. *J. Geophys. Res., .*
- Kikuchi, K., and Takayabu, Y. (2004). The development of organized convection associated with the MJO during TOGA COARE IOP: Trimodal characteristics. *Geophysical Research Letters, 31.*
- Koch, D., Jacob, D., and Graustein, W. (1996). Vertical transport of tropospheric aerosols as indicated by  $^{7}\text{Be}$  and  $^{210}\text{Pb}$  in a chemical tracer model. *J. Geophys Res., 101, 18,651–18,666.*
- Koch, D. M., and Mann, M. E. (1996). Spatial and temporal variability of  $^{7}\text{Be}$  surface concentrations. *Tellus B, 48, 387–396.*
- Lal, D., and Peters, B. (1967). Cosmic ray produced radioactivity on the earth. In K. Sitte (Ed.), *Handbuch der Physik* (pp. 551–612). Springer-Verlag volume 46.
- Lawrence, M. G., and Rasch, P. J. (2005). Tracer transport in deep convective updrafts: plume ensemble versus bulk formulations. *J. Atmos. Sci., 62, 2880–2894.*
- Le Treut, H., and Li, Z.-X. (1991). Sensitivity of an atmospheric general circulation model to prescribed sst changes: feedback effects associated with the simulation of cloud optical properties. *Climate Dynamics, 5, 175–187.*
- Liu, H., Jacob, D., Bey, I., and Yantosca, R. (2001). Constraints from  $^{210}\text{Pb}$  and  $^{7}\text{Be}$  on wet deposition and transport in a global three-dimensional chemical tracer model driven by assimilated meteorological fields. *J. Geophys Res., 106, 12,109–12,128.*
- Mahowald, N. M., Rasch, P. J., and Prinn, G. R. (1995). Cumulus parameterizations in chemical transport models. *J. Geophys Res., 100, 26,173–26,189.*
- Marley, N. A., Gaffney, J. S., Drayton, P. J., Cunningham, M. M., Orlandini, K. A., and Paode, R. (2000). Measurement of  $^{210}\text{pb}$ ,  $^{210}\text{po}$ , and  $^{210}\text{bi}$  in size-fractionated atmospheric aerosols: An estimate of fine-aerosol residence times. *Aerosol Science and Technology, 32, 569–583.*
- Mircea, M., Stefan, S., and Fuzzi, S. (2000). Precipitation scavenging coefficient: influence of measured aerosol and raindrop size distributions. *Atmospheric Environment, 34, 5169 – 5174.*
- Preiss, N., and Genthon, C. (1997). Use of a new database of lead 210 for global aerosol model validation. *J. Geophys. Res., 102, 25347.*
- Pruppacher, H., and Klett, J. (1996). *Microphysics of Clouds and Precipitation.* Atmospheric and Oceanographic Sciences Library. Springer.
- Radke, L. F., Hobbs, P. V., and Eltgroth, M. W. (1980). Scavenging of aerosol particles by precipitation. *J. Appl. Meteor, 19, 715–722.*
- Rasch, P. J., Feichter, J., Law, K., Mahowald, N., Penner, J., Benkovitz, C., Genthon, C., Giannakopoulos, C., Kasibhatla, P., Koch, D., Levy, H., Maki, T., Prather, M., Roberts, D. L., Roelofs, G.-J., Stevenson, D., Stockwell, Z., Taguchi, S., Kritz, M., Chipperfield, M., Baldocchi, D., McMurry, P., Barrie, L., Balkanski, Y., Chatfield, R., Kjellstrom, E., Lawrence, M., Lee, H. N., Lelieveld, J., Noone, K. J., Seinfeld, J., Stenchikov, G., Schwartz, S., Walcek, C., and Williamson, D. (2000). A comparison of scavenging and deposition processes in global models: results from the WCRP Cambridge workshop of 1995. *Tellus B, 52, 1025–1056.*
- Reddy, S., and Boucher, O. (2004). A study of the global cycle of carbonaceous aerosols in the LMDZT general circulation model. *J. Geophys. Res., 109.*
- Salzmann, M., Lawrence, M. G., Phillips, V. T. J., and Donner, L. J. (2004). Modelling tracer transport by a cumulus ensemble: lateral boundary conditions and large-scale ascent. *Atmospheric Chemistry and Physics, 4, 1797–1811.*
- Schulze, J., Auer, M., and Werzi, R. (2000). Low level radioactivity measurement in support of the CTBTO. *Applied Radiation and Isotopes, 53, 23 – 30.*
- Shapiro, M., and Forbes-Resha, J. (1976). Mean residence time of  $^{7}\text{Be}$ -bearing aerosols in the troposphere. *J. Geophys Res., 81, 2647–2649.*
- Slinn, W. G. N. (1983). Precipitation scavenging. In D. Raderson (Ed.), *Atmospheric Sciences and Power Production Chapter 11.* Division of Biomedical Environmental Research, US Department of Energy.
- Sportisse, B. (2007). A review of parameterizations for modelling dry deposition and scavenging of radionuclides. *Atmospheric Environment, 41, 2683–2698.*
- Tost, H., Jöckel, P., and Lelieveld, J. (2006). Influence of different convection parameterisations in a GCM. *Atmospheric Chemistry and Physics Discussions, 6, 9213–9257.*
- Tost, H., Lawrence, M. G., Brühl, C., Jöckel, P., and Team, T. G. (2010). Uncertainties in atmospheric chemistry modelling due to convection parameterisations and subsequent scavenging. *Atmospheric Chemistry and Physics, 10, 1931–1951.*
- Winkler, R., Dietl, F., Frank, G., and Tschiersch, J. (1998). Temporal variation of  $^{7}\text{Be}$  and  $^{210}\text{Pb}$  size distributions in ambient aerosol. *Atmospheric Environment, 32, 983 – 991.*
- Yanai, M., Chen, B., and Tung, W.-w. (2000). The Madden-Julian oscillation observed during the TOGA COARE IOP: Global view. *J. Atmos. Sci., 57, 2374–2396.*
- Yoshimori, M. (2005). Beryllium 7 radionuclide as a tracer of vertical air mass transport in the troposphere. *Advances in Space Research, 36, 828 – 832.*